Article:
Bačová, P, Lentzakis, H, Read, DJ et al. (3 more authors) (2014) Branch-point motion in architecturally complex polymers: estimation of hopping parameters from computer simulations and experiments. Macromolecules. ISSN 0024-9297

https://doi.org/10.1021/ma5003936

Branchpoint motion in architecturally complex polymers: estimation of hopping parameters from computer simulations and experiments

Petra Bačová,[†] Helen Lentzakis,[‡,¶] Daniel J. Read,[§] Angel J. Moreno,[*,†,‖] Dimitris Vlassopoulos,[‡,¶] and Chinmay Das[⊥]

Centro de Física de Materiales (CSIC, UPV/EHU) and Materials Physics Center MPC, Paseo Manuel de Lardizabal 5, E-20018 San Sebastián, Spain, Foundation for Research and Technology Hellas (FORTH), Institute of Electronic Structure & Laser, Heraklion, Crete 71110, Greece, Univerisity of Crete, Department of Materials Science and Technology, Heraklion, Crete 71300, Greece, Department of Applied Mathematics, University of Leeds, LS2 9JT Leeds, UK, Donostia International Physics Center, Apartado 1072, 20080 San Sebastián, Spain, and School of Physics and Astronomy, University of Leeds, Leeds LS2 9JT, United Kingdom

E-mail: wabmosea@ehu.es

Abstract

[*]To whom correspondence should be addressed

[†]Centro de Física de Materiales (CSIC, UPV/EHU) and Materials Physics Center MPC, Paseo Manuel de Lardizabal 5, E-20018 San Sebastián, Spain

[‡]Foundation for Research and Technology Hellas (FORTH), Institute of Electronic Structure & Laser, Heraklion, Crete 71110, Greece

[¶]Univerisity of Crete, Department of Materials Science and Technology, Heraklion, Crete 71300, Greece

[§]Department of Applied Mathematics, University of Leeds, LS2 9JT Leeds, UK

[‖]Donostia International Physics Center, Apartado 1072, 20080 San Sebastián, Spain

[⊥]School of Physics and Astronomy, University of Leeds, Leeds LS2 9JT, United Kingdom

Relaxation of branched polymers under tube based models involve a parameter p^2 characterizing the hop-size of relaxed side-arms. Depending on assumptions made in rheological models (e.g. about the relevant tube diameter for branchpoint hops) p^2 had been set to values varying from 1 to 1/60 in the literature. From large-scale molecular dynamics simulations of melts of entangled branched polymers of different architectures, and from experimental rheological data on a set of well-characterized comb polymers with many (~ 30) side-arms, we estimate the values of p^2 under different assumptions in the hierarchical relaxation scheme. Both the simulations and the experiments show that including the backbone friction and considering hopping in the dilated tube provides the most consistent set of hopping parameters in different architectures.

1 Introduction

Over the last years, experimental studies on branched polymers have gone hand in hand with theoretical work aiming to explain their exceptional viscoelastic properties.[1–4] While the viscoelasticity of linear chains is well described by the tube theory,[5] entangled branched polymer melts reveal a more complex dynamic behavior as a consequence of their complicated structure.[6] All of them include one branchpoint (in the case of stars) or more (H-polymers, combs, Cayley trees, hyperbranched etc.), which dramatically slow down the overall relaxation of the material. The slow relaxation processes are reflected in the rheological spectrum, extending over several time decades, and play an important role during industrial processing.[7] A correct implementation of the branchpoint dynamics in tube-based models seems to be essential for accurate theoretical predictions of the rheological properties of these materials.

Molecular segments in the entanglement network of branched polymers relax hierarchically, progressing from the outer to the inner parts of the molecule. The arms are retracted back and forward along the tubes and their retraction becomes less favorable as the branchpoint is approached.[8] This leads to an exponential distribution of the relaxation times along the arm, and to a progressive dilution of the entanglement network. At times longer than the relaxation time of outer segments,

inner segments do not experience the entanglements with the outer ones, which have relaxed at much earlier time scales. As a result, the original tube becomes wider ('dilated tube') with time. This mechanism is known as dynamic tube dilution (DTD).[9,10] Once the arms are fully relaxed, they act as sources of additional friction, i.e., as frictional 'fat beads'. The branchpoint at these time scales probes the space liberated by the removed constraints of the arm, and performs diffusive steps (hops) along the tube contour with a diffusivity given by:

$$D = \frac{p^2 a^2}{2\tau_a} \tag{1}$$

where τ_a is the longest relaxation time of the arm and a is the tube diameter. This may be the original or the dilated one (see below). In the following the symbol a will be used for the dilated tube. The original, undilated, tube diameter will be denoted as a_0. In the case of asymmetric structures (e.g., T- and Y-shaped stars, combs, etc), the branched architecture is reduced to an effective linear chain containing the frictional beads representing the relaxed short arms. At this point, the final stage of the relaxation is mediated by reptation of the backbone. In symmetric structures (symmetric stars, Cayley trees...) reptation is not possible, and after retraction of the main arms all stress is considered to be relaxed; hopping of the central branchpoint is the only available mechanism for later motion.

The factor p^2 in equation Eq. (1) is a dimensionless constant called the hopping parameter. Thus, it is assumed that the typical hopping distance is p times the tube diameter, and that hopping occurs every time the arm relaxes. Naively, it may be expected that p^2 is of the order of unity. However, a series of investigations have suggested considerably smaller values in the case of asymmetric T-shaped stars with weakly or moderately entangled short arms. This was first pointed out by Frischknecht *et al.*[11] They found that, in order to reproduce the experimental rheological data with hierarchical tube-based models, the value of p^2 needed to be adjusted depending on the length of the short arm. The values obtained in Ref.[11] varied in the range $1/4 \leq p \leq 1/60$. The smaller the short arm was, the lower value of p^2 was needed, decreasing (through equation Eq. (1)) the

corresponding diffusivity compared to the naive value for $p^2 = 1$. Thus, the relaxed short arms in the asymmetric stars caused much more drag than expected, even in the case of very weakly entangled short arms. Chen and Larson analyzed, in combination with hierarchical models, rheological data of asymmetric stars with the same length of the short arm, but this being linked at different positions along the backbone (forming T-shaped or Y-shaped stars).[12] They described the experimental data by using a fixed hopping parameter $p^2 = 1/12$. We note that an alternative tube-model approach, the time marching algorithm (TMA) uses $p^2 = 1$ but invokes different molecular assumptions which in essence (implicitly) require a different friction due to the branch point. So, for example, in TMA, reptation is determined by considering the length of the primitive path of the whole backbone (not only of the unrelaxed fraction of the backbone, as in the BoB[3] or hierarchical models[2]).

Branchpoint motion has also been characterized in more complex branched architectures. McLeish *et al.*[13] found the value $p^2 = 1/12$ to account well for rheological data of H-polymers.[14] Further experimental studies generalized the approach for H-polymers of Ref.[13] to the case of comb polymers. Daniels *et al.*[15] kept the value of the hopping parameter $p^2 = 1/12$ and analyzed the possible factors affecting the rheological spectra. They studied the change in the dynamics with increasing number of arms in the comb structure. Some authors incorporated the effect of the different length of the free backbone ends and side arms .[16,17] As previously found for their star-like counterparts,[11,18] rheological experiments of comb polymers with short, weakly entangled, branches revealed that these exerted a higher frictional drag than expected.[19] Kirkwood *et al.* proposed to solve this problem by fixing again the value $p^2 = 1/12$ and using a different, effective entanglement length for the branches.[19]

Further investigations have shown that reduced values of $p^2 \ll 1$ are universally found for branched architectures with weakly entangled short side arms, the values being strongly dependent on the arm length.[20–22] On the other hand, recent studies on comb polymers using the TMA, have kept the original value of the hopping parameter, $p^2 = 1$, as already mentioned, and used a different molecular coordinate system accounting for the entire original backbone.[23] In addition, we note

that the effects of architectural dispersity have been recently considered and analyzed.[24–26]

There have been only a few theoretical attempts to specify *a priori* the value of p^2. Lee *et al.*[20,27] extended hierarchical tube models to include branchpoint diffusion in a self-consistent way, accounting for linear rheology of Y-shaped asymmetric stars, combs and pom-pom molecules. The hopping parameter was identified as $p^2 = 1/Z_{AR}$ being independent of the specific architecture, with Z_{AR} the entanglement density of the unrelaxed backbone segments at the hopping events. Some studies using slip-link simulations have focused on the nature of the branchpoint motion itself. Shanbhag and Larson [28] suggested that the branchpoint diffusion is limited by the *full* removal of the entanglements around the short arm. Masubuchi *et al.*[29] examined the relaxation mechanisms of the branchpoint and their contribution to the viscoelastic relaxation of asymmetric stars. They observed that the more asymmetric the structure is, the more relevant the contribution of branchpoint hopping becomes for the overall relaxation of the star.

The above review of the literature reveals that there are a very large range of values reported for the hopping parameter p^2. Why is this? We consider that there are two separate causes, as follows.

Firstly, there are different assumptions made about the branchpoint hopping process itself, within the context of dynamic dilution theory. These assumptions are about two aspects of the hopping: i) the length-scale associated with hops– this might be set by the original ("thin") tube diameter or dilated ("fat") tube diameter, and ii) the direction, or path, of the hopping motion– hops may be considered to occur along the paths of the thin tube contour or fat tube contour. Different versions of hierarchical tube-based models make different choices on these two characteristics of the branchpoint hopping motion.[11,15–17,19,22,30]

Secondly, the appropriate value of p^2 is normally determined by inference from rheological data, rather than by measuring the branchpoint motion directly. The data are interpreted by making use of a suitable (hierarchical) rheological model. In addition to the above assumptions made about the hopping process itself, such models encode further assumptions about polymer relaxation,[3,4,31] for example in the mathematical description of deep contour length fluctuations. See, e.g., the discussion in Ref.[32] As a result, inferences made about the rate of branchpoint diffusion

are themselves dependent on the model used to interpret the data. So, it is quite possible that this process deduces the wrong rate of branchpoint diffusion (because the branchpoint motion is not measured directly) which is then interpreted using the wrong assumptions for the hopping process. It is therefore not surprising that a wide range of numerical values for p^2 ensue.

Given the wide range of assumptions on branchpoint hopping introduced by hierarchical models, we aim in this article to address a fundamental issue: can we rule out some of these assumptions? We present a critical analysis of the consistency of the different assumptions for branchpoint hopping. We perform large-scale molecular dynamics (MD) simulations on several branched architectures. These include symmetric stars, asymmetric T-shaped and Y-shaped stars, combs and mixtures of stars and linear chains. The MD simulations allow us to analyze directly the diffusive motion of the branchpoints, rather than make inferences from rheology data. We also analyze friction of the branchpoints and tube dilution. Using these data, we determine p^2-values for each set of specific assumptions for branchpoint hopping.

Since our aim is to rule out some of these assumptions, we state in advance our criterion for deciding what is a "good" assumption, and what is a poor one. Our criterion is simple, and based on the requirement of a universal behavior: a good set of assumptions should result in broadly similar values of p^2 across the different systems studied. So, if a specific assumption regarding branchpoint hopping requires very different values of p^2 to model the branchpoint diffusion of different systems, then that particular assumption will be ruled out by this exercise. Then, having arrived at an optimal set of assumptions, we can go on to ask what typical value of p^2 should be used. Throughout this exercise, we shall pay particular attention to errors in determining the different physical quantities measured by the simulations. Where possible, we aim to estimate quantities by more than one method, as a check on the consistency of our results. This allows us to decide whether differences in the p^2-values obtained for different simulations are significant, or within reasonable error bounds.

As a final check on our conclusions, we discuss simulation results in comparison with linear rheological data of well-characterized comb polymers with weakly or moderately entangled

branches. This type of experimental system was chosen for several reasons: (i) the large number of side arms means that there is a discernible experimental signal of the arm relaxation in the linear rheology data, allowing an experimental estimate to be made of the arm relaxation time, and (ii) following relaxation of the side arms, the combs are geometrically simple (linear) objects, and so the terminal relaxation can be analyzed using reptation theory. Thus, while direct experimental measurement of branchpoint motion is not possible we can at least make an estimate of the motion without resorting to one of the more complicated hierarchical models. In what follows, we discuss our analysis of the experimental system in parallel with the simulation results because there are some similarities in the analysis, for example difficulties in estimating the arm relaxation time, and the need to use several different methods as a check on consistency.

The article is organized as follows: in Section 2 we present the simulated systems of branched polymers, we describe the simulated model and give simulation details. In Section 3 we summarize the main theoretical predictions for branchpoint motion. This section introduces equations related to branchpoint motion that are later used for obtaining p^2 of the simulated and experimental systems. In Section 4 and Section 5 we estimate the variables figuring in the equations in Section 3 for different molecular architectures, by analyzing simulation and rheological data, respectively. Subsequently, we use the obtained variables to calculate the values of p^2 for both the simulated and experimental systems. Results are summarized and discussed in Section 6. Conclusions are given in Section 7.

2 Simulation details

The branched polymers in our MD simulations were modeled by the bead-spring Kremer-Grest model.[33] Monomeric units are coarse-grained into beads with diameter σ, mass m_0 and excluded volume represented by a repulsive Lennard-Jones (LJ) potential:

$$U_{\mathrm{LJ}}(r) = \begin{cases} 4\varepsilon \left[\left(\frac{\sigma}{r}\right)^{12} - \left(\frac{\sigma}{r}\right)^{6} + \frac{1}{4} \right] & \text{for } r \leq r_{\mathrm{c}}, \\ 0 & \text{for } r > r_{\mathrm{c}}, \end{cases} \tag{2}$$

with cut-off distance $r_c = 2^{1/6}\sigma$. Bonded beads are connected by springs, introduced as a finite-extension nonlinear elastic (FENE) potential:

$$U_F = -\frac{1}{2}K_F R_F^2 \ln\left[1 - \left(\frac{r}{R_F}\right)^2\right], \tag{3}$$

with spring constant $K_F = 30\varepsilon/\sigma^2$ and maximum spring length $R_F = 1.5\sigma$. In addition to the original Kremer-Grest interactions, we applied a bending potential given by:

$$U_{bend}(\theta) = k_\theta(1 - \cos\theta), \tag{4}$$

where θ is the angle between three consecutive beads ($\theta = 0$ for a rod). A bending constant $k_\theta = 2\varepsilon$ was imposed to increase slightly the stiffness of the chains. The resulting characteristic ratio at the simulated density and temperature (see below) is $C_\infty = 3.68$. This choice was made to decrease the value of the entanglement length in comparison to that of the flexible chains ($k_\theta = 0$).[34] In the following we assume a nominal value of the entanglement length of $N_e \approx 25$. This value is the average of $N_e^{PP} = 23$ and $N_e^{MSD} = 27$, these being estimated by analysis of the primitive path[35] and monomer mean square displacement,[18] respectively. In the following we will use the diameter σ as the length unit, and time will be expressed in units of $\tau_0 = (m_0\sigma^2/\varepsilon)^{1/2}$. The corresponding entanglement time τ_e for our model is $\tau_e = 1800\tau_0$.[18]

The simulated systems are illustrated in Figure 1. These include symmetric stars, T- and Y-shaped asymmetric stars, combs, and mixtures of T-stars with linear chains. Red labels denote the number of entanglements per arm in each architecture (by using the nominal value $N_e = 25$ beads per entanglement segment, as mentioned before). See figure caption for details. The simulated architectures and used values for the arm lengths have been selected to investigate several effects on the dynamics, namely: i) the effect of the short-arm length for a fixed architecture (881, 882, 883 and 888 systems), ii) the effect of the branchpoint position for stars with identical backbones and short arms (882 and Y4212 systems), iii) the effect of adding an identical, short arm to an asymmetric star (Y4212 vs. comb), iv) the effect of diluting the entanglement network by mixing

with weakly entangled linear chains (883 vs. mix11 and mix21 systems).

All the systems were simulated, by using the ESPResSo package,[36] at number density $\rho = 0.85\sigma^{-3}$ and temperature $T = \varepsilon/k_{\mathrm{B}}$, with k_{B} the Boltzmann constant. The number of beads in the simulation box for the different investigated systems ranged from 75300 to 107100 (see details in Figure 1). The polymers were first constructed by joining building blocks that were sampled from simulations of unentangled stars and linear chains with the same interactions of Eq. (2)-Eq. (4). The angles at the junction points between building blocks were chosen in order to obtain the correct distribution of intramolecular distances (see Ref.[37] for details). Once the polymers were constructed and randomly inserted in the simulation box, we equilibrated the system. The equilibration protocol, based on the method of Auhl *et al.*[37] consisted of three steps: i) a Monte Carlo run for prepacking of rigid macromolecules, ii) an MD run for progressive introduction of excluded volume by capped LJ interactions ('slow push-off'), and iii) a further equilibration MD run with the full interactions. A detailed description of the protocol can be found in Ref.[38] After equilibration, production MD runs were performed, extending over typically one to five billion MD steps. The MD runs were integrated by using the velocity-Verlet algorithm with time step $\Delta t = 0.01\tau_0$. The temperature in the MD runs was controlled by the Langevin thermostat with a friction constant $\Gamma = 0.5m_0/\tau_0$.

3 Diffusion of the branchpoint: theoretical background

After the relaxation of the short arm, this effectively acts as a frictional 'fat bead'. Consequently the backbone, which in the case of the asymmetric stars is formed by the two long arms, is able to reptate. The branch point motion at these time scales can be seen as a curvilinear diffusion along a tube of diameter a. The trajectory of the branch point is assumed to be a random walk,

$$\langle r^2 \rangle = |L|a, \tag{5}$$

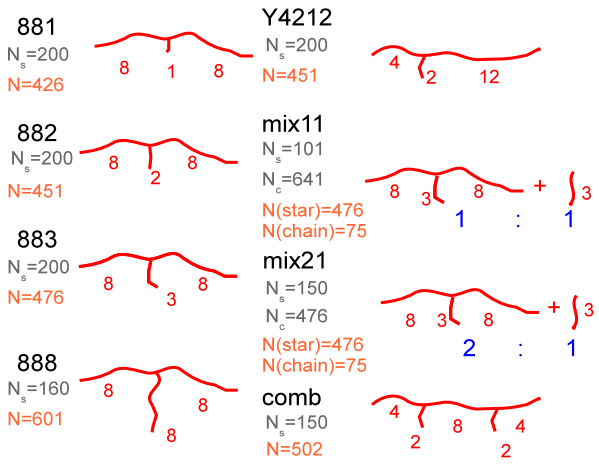

Figure 1: Schematic representation of the simulated systems. The numbers at each arm denote the number of entanglements in the arm, by using the nominal value of $N_e = 25$ beads per entanglement segment (see above). In the rest of the paper the different simulated systems will be denoted according to the big labels. The simulated systems include: i) asymmetric T-shaped stars (881, 882, 883), ii) asymmetric Y-shaped stars (Y4212), iii) symmetric stars (888), iv) comb polymers, and v) mixtures of 883-stars with linear chains. The fraction of beads in the simulation box that belong to the stars is 1/2 in the mixture 'mix11' and 2/3 in the mixture 'mix21'. The labels 1:1 and 2:1 denote such relative compositions. N_s denote the total number of stars in the simulation box, N_c denote the number of linear chains in the mixtures. N represents the total number of beads per macromolecule.

where $\langle r^2 \rangle$ is the mean square distance between the start and end points of the trajectory, and $|L|$ is the length of the primitive path that is explored by the branch point in this trajectory. A Gaussian distribution is assumed for the diffusion length L. Therefore, Eq. (5) can be expressed as

$$\langle r^2 \rangle = \frac{2a}{\sqrt{2\pi \langle L^2 \rangle}} \int_0^\infty L \exp\left(\frac{-L^2}{2\langle L^2 \rangle}\right) \mathrm{d}L, \tag{6}$$

which leads to the relation:

$$\langle r^2 \rangle = a\sqrt{2\langle L^2 \rangle / \pi}. \tag{7}$$

Since we have assumed a diffusive motion of the branch point along the primitive path, we can relate $\langle L^2 \rangle$ and the diffusivity D as

$$\langle L^2 \rangle = 2Dt \tag{8}$$

where the factor 2 results from the one-dimensional character of the curvilinear diffusion. From Eq. (7) and Eq. (8) we find:

$$D = \frac{\pi}{4a^2}\left(\frac{\langle r^2\rangle}{t^{1/2}}\right)^2. \tag{9}$$

Eq. (9) provides a direct way of obtaining the diffusivity for the curvilinear, reptative motion of the branchpoint. In the reptative regime the mean squared displacement will scale as[5] $\langle r^2\rangle \propto t^{1/2}$. Therefore, by obtaining from the simulations the corresponding plateau value of the ratio $\langle r^2\rangle/t^{1/2}$, the diffusivity can be easily calculated. We note here that when dynamic tube dilution is included, there are different tube diameters that could be considered. There are a set of nested tubes, each of which is parameterised by its tube diameter, a. As written, Eq. (9) gives the effective diffusion constant for the random motion of the branchpoint, when this motion is mapped onto the path for the tube with diameter a. Thus a particular motion (giving rise to a plateau value of $\langle r^2\rangle/t^{1/2}$) can be construed either as rapid diffusion along a tube path with a small tube diameter, or as slower motion along a shorter tube path with a larger tube diameter.

As mentioned in the Introduction, the branchpoint is assumed to hop in the tube every time the short arm relaxes (Eq. (1)). This branchpoint hopping may occur in the skinny (a_0) or in the dilated (a) tube. In order to investigate both possible cases, we modify Eq. (1) in the way it was done in eq. 11 of Ref.:[3]

$$D = \frac{p^2 a_h^4}{2q\tau_a a^2}. \tag{10}$$

The parameter a_h denotes the tube diameter (a_0 or a) in which the branchpoint hopping takes place. In deriving Eq. (10), Ref.[3] assumes that the length a_h sets both (i) the typical distance of the hops, and (ii) the tube contour along which the hops take place. This is then converted to an effective diffusion constant D, for motion mapped on to the tube path set by tube diameter a. We note that, if Eq. (9) and Eq. (10) are equated then the factor a^2 cancels: the large scale motion given by $\langle r^2\rangle/t^{1/2}$ will depend only on the tube diameter a_h within which hops take place. We equate Eq. (9) and Eq. (10) below if we assume that branchpoint friction dominates the motion. This is to be contrasted with, for example, Frischknecht *et al.*,[11] who (when considering hops in a

skinny tube) sometimes consider the length of the hop to be set by a_0, but the path of the hop to be along the dilated tube contour.

Eq. (10) includes an additional factor q. The factor q is the number of side arms attached to the main backbone ($q = 1$ for the stars, $q = 2$ for the simulated combs), and it is introduced for accounting for all frictional contributions from the relaxed q short arms. In the case $a_h = a$ and $q = 1$, Eq. (10) reduces to the original Eq. (1).

As mentioned in the Introduction, the hopping parameter p^2 used in the expression for the branchpoint diffusivity was experimentally found to be considerably smaller than unity, reflecting a stronger drag from relaxed arms than expected. A possible explanation is that Eq. (1) and Eq. (10) overestimate the diffusivity by missing the friction contribution from the chain itself. We attempt to correct this point by adding the chain friction for the motion along the skinny tube, allowing for a rescaling to the dilated tube in the manner of eq. 36 of Ref.[39] The corresponding equation for the diffusivity reads:

$$D = \left(\frac{3\pi^2 \tau_e Z}{\phi^\alpha a_0^2} + \frac{2q\tau_a a^2}{p^2 a_h^4} \right)^{-1}, \tag{11}$$

where Z is the number of entanglements along the backbone, a_0 is the undilated tube diameter, τ_e is the entanglement time, and ϕ^α represents the fraction of material giving rise to slow constraints (see below). As discussed in detail in Ref.[39] (building on the earlier work of Viovy *et. al*[40]), the factor ϕ^α in the first term on the right hand side of Eq. (11) arises because the 'solvent' (giving the dilated tube) is actually formed by slow moving entangled chains. The fastest mode for diffusion along the dilated tube is *via* chain motion along the skinny tube. Motion directly along the dilated tube requires many constraint release events and is therefore much slower. The factor ϕ^α is due to projecting chain motion along the skinny tube onto the shorter diluted tube path.

For the mixtures of asymmetric 883-stars (see Figure 1) and linear chains, constraint release from the solvent (the short, linear chains) is a little faster, and we can refine equation Eq. (11) to allow for chain motion along the dilated tube, mediated by this constraint release (see eq. 39 of

Ref.[39]):

$$D = \left(\frac{3\pi^2 \tau_e Z}{a_0^2} \left[\phi^\alpha + \left(\frac{2}{3\pi^2 \nu \tau_e} + \frac{1}{1-\phi^\alpha} \right)^{-1} \right]^{-1} + \frac{2\tau_a a^2}{p^2 a_h^4} \right)^{-1}, \tag{12}$$

where $\nu = c_\nu \tau_s^{-1}$ is the constraint release rate from the linear chains in the mixture, τ_s is their relaxation time and c_ν is the rate constant. In Eq. (12) we have dropped the factor q since for the 883-stars $q = 1$. We note that, in the limit of extremely fast constraint release ($\nu \to \infty$) the friction for chain motion along the dilated tube becomes independent of ϕ^α. In practice, even for the mixtures with short linear chains, Eq. (12) gives only a small correction to Eq. (11).

Again, we contrast Eq. (11) and Eq. (12) with the work of Frischknecht *et al.*[11] When considering reptation of the backbone along the dilated tube, they assumed that the only friction experienced by the backbone was the monomeric (or "Rouse") friction. This neglects the fact that, for chain motion along the dilated tube, constraint release events need to occur, and these give rise to drag on the chain. Here we consider two possibilities: that the constraint release events are so slow, the fastest motion available to the chain is along the skinny tube, but subject to monomeric friction - this gives Eq. (11). For the blends, we also consider including constraint release events approximated to be at a fixed rate - this gives Eq. (12). The work of Frischknecht *et al.* corresponds to Eq. (12) in the limit $\nu \to \infty$. Thus, in using Eq. (11) and Eq. (12), together with hopping in a dilated tube, we are considering an option not used by Frischknecht *et al.*, namely branchpoint hopping in the dilated tube, but backbone motion dominated by movement along the skinny tube. Finally, if we know the tube diameter and use the simulation value for the reptation plateau in $\langle r^2 \rangle / t^{1/2}$, we can obtain the hopping parameter p^2 by combining Eq. (9) with one of the Eq. (10), Eq. (11), Eq. (12).

Once we have presented equations for branchpoint motion in the simulated systems, we draw our attention to experiments. We will focus on the illustrative case of experimental comb polymers. Regarding the analysis of the experimental combs, we have no direct access to the diffusivity D. Therefore, we proceed in a related but different manner to obtain p^2. As in the other asymmetric architectures, the combs relax as effective linear chains (by reptation) after the relaxation of the

short side arms. Likewise, reptation can be considered in a dilated tube (but with an enhanced friction), due to the faster dynamics of the entanglements of the backbone with short side arms. For each comb, we can deduce the number of effective entanglements, Z_{dil}, in the dilated tube as:

$$Z_{dil} = Z_b \frac{Z_b}{Z_b + qZ_a}, \tag{13}$$

where Z_b and Z_a are the number of entanglements along the backbone and at each of the q side arms, respectively. With this, the effective relaxation time $\tau_{e,dil}$ of a diluted entanglement segment can be obtained as:

$$\tau_{e,dil} = \tau_d / r_{dil}, \tag{14}$$

where τ_d is the *experimentally* measured terminal time of the comb, and r_{dil} is the ratio of the terminal to the entanglement time of the linear chain with the same number of entanglements, Z_{dil}, as the diluted comb. This ratio can be calculated from the Likhtman-McLeish theory for linear chains as:[41]

$$r_{dil} = \frac{\tau_d^{lin}}{\tau_e^{lin}} = 3Z_{dil}^3 \left(1 - \frac{3.38}{Z_{dil}^{1/2}} + \frac{4.17}{Z_{dil}} - \frac{1.55}{Z_{dil}^{3/2}}\right). \tag{15}$$

In applying Eq. (15) to combs, we are assuming that the combs behave exactly as rescaled linear polymers in their terminal relaxation. In particular, we assume that the depth of contour length fluctuations is commensurate with the diluted tube (c.f. the binary blend case in Ref.[39]). We also assume that the rate of contour length fluctuations and terminal reptation are rescaled by exactly the same time constant (i.e. slowed down compared to the corresponding linear chain by the large contribution of side arm friction). Thus, the effective rescaled entanglement time $\tau_{e,dil}$ includes contributions from side arm friction, just as the experimentally measured terminal time τ_d includes the side arm friction. So, the diffusion constant we derive below (Eq. (16)) is the effective diffusion constant along the diluted tube, including contributions from the side arm friction.

For a linear chain, the entanglement time and curvilinear diffusivity are given respectively by $\tau_e = \zeta N_e^2 b^2/(3\pi^2 k_B T)$ and $D = k_B T/(\zeta Z N_e)$, where N_e is the total number of monomers per entanglement segment, ζ is the microscopic bare friction and b is the Kuhn segment length.[5]

Moreover $a_0^2 = N_e b^2$ due to Gaussianity. By combining the former expressions, the diffusivity is given by $D = a_0^2/(3\pi^2\tau_e Z)$. In the reptative regime of the combs, this relation holds for the diluted number of entanglements ($Z \to Z_{dil}$), dilated tube ($a_0 \to a$), and the effective relaxation time of the diluted entanglement segment ($\tau_e \to \tau_{e,dil}$):

$$D = \frac{a^2}{3\pi^2 \tau_{e,dil} Z_{dil}}. \tag{16}$$

Thus, our procedure is as follows. We measure, experimentally, the terminal time τ_d of the combs. Using Eq. (14) and Eq. (15), this allows us to obtain the effective entanglement time $\tau_{e,dil}$ for the comb, treating it as a renormalised linear chain. Then, Eq. (16) gives our experimental estimate of the effective diffusion constant for the comb along the diluted tube contour, which we compare with Eq. (10), Eq. (11) or Eq. (12) as appropriate. The number of side arms in the experimental combs is very large (see Section 5). Therefore, in this case we can neglect the contribution from the backbone friction and we just use, in combination with Eq. (16), the simple Eq. (10) to calculate p^2. On the other hand, the simulated comb has only two side arms and the backbone friction may play an important role. In this case we combine Eq. (9) with Eq. (11).

The equations presented in this section establish a direct relation between p^2 and several observables that can be directly measured from the simulation and experimental information. We determine this information in Section 4 (simulations) and Section 5 (experiments), and use it for obtaining the corresponding p^2-values in Section 6.

4 Analysis: simulations

4.1 Branchpoint displacement

The plateau value of $\langle r^2(t)\rangle/t^{1/2}$ for Eq. (9) can be directly obtained from the simulation data, by analyzing the time evolution of the mean square displacement (MSD, $\langle r^2(t)\rangle$) of the branchpoint. However, this MSD has poor statistics because of the limited number of branchpoints in the simulation box. In order to improve statistics considerably, without significant effects in the results, we

have averaged the MSD of the 'branchpoint' over ten beads: the actual branchpoint and the three nearest consecutive beads at each of the three arms stemming from the branchpoint. Figure 2 shows the so-obtained values divided by $t^{1/2}$, for the different investigated systems. At long time scales, beyond $t \sim 10^6 - 10^7$ depending on the system, all the data exhibit a plateau, except for the case of the symmetric stars. This result suggests that asymmetric stars and combs relax in such time scales by reptation, with the MSD showing the well-known power-law behavior $\langle r^2(t)\rangle \propto t^{1/2}$ for reptating linear chains.[5] For symmetric stars relaxation is exclusively mediated by arm retraction. Hence no plateau in $\langle r^2(t)\rangle / t^{1/2}$ is expected to arise at time scales beyond the simulation window.

In order to obtain a reliable value of the plateau for Eq. (9), we average the simulation data of $\langle r^2(t)\rangle / t^{1/2} \propto t^0$ for times $t > 5 \times 10^6$, where the plateau is well resolved. The so-obtained values are indicated as horizontal lines in Figure 2, and are listed in Table 2.

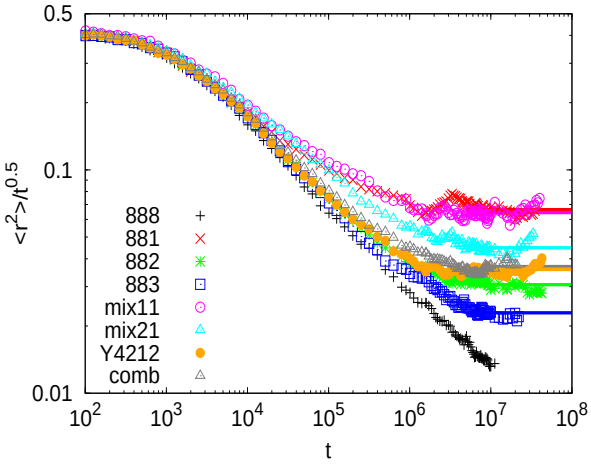

Figure 2: Symbols: MSD of the branchpoint divided by $t^{1/2}$, for all the investigated systems. The solid lines for each data set represent the average value of $\langle r^2(t)\rangle / t^{1/2}$ over the long-time plateau.

4.2 Relaxation times

In this subsection we determine the longest relaxation time, τ_a, of the short arm. For this, we analyze its end-to-end correlation function. This is defined as:

$$C(t) = \frac{\langle \mathbf{P}(t) \cdot \mathbf{P}(t_0)\rangle}{P^2(t_0)}, \tag{17}$$

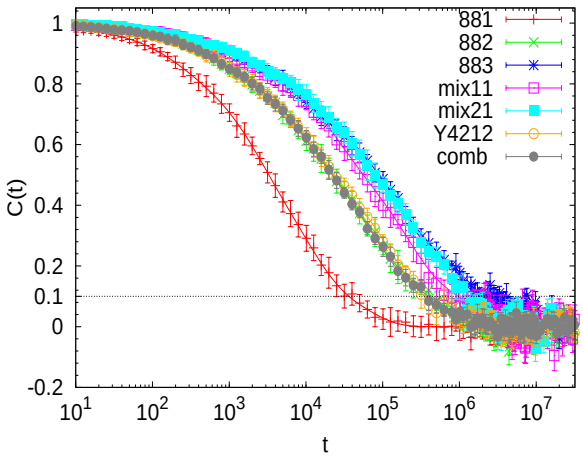

Figure 3: End-to-end correlators of the short arms for the different simulated systems. Symbols with error bars are simulation data. Solid lines are fits to a weighted sum of exponentials (Eq. (18)). The dotted line indicates the upper level of noise.

where $\mathbf{P}(t), \mathbf{P}(t_0)$ is the end-to-end vector of the short arm at times t and t_0 respectively. When the correlation function decays to 0 the short arm is fully relaxed. We show the correlation functions of all the simulated systems in Figure 3. For each system we computed the end-to-end correlator for 15 equispaced uncorrelated time origins t_0. Each data set in Figure 3 is the average over the corresponding 15 correlators. The error bars indicate, for each time t, the respective upper and lower value obtained in the 15 correlators. In order to describe accurately the decay of the end-to-end correlator and to get a reliable value of τ_a, we fitted the simulation data of Figure 3 to several empirical functions. The stretched exponential Kohlrausch-William-Watts (KWW) function, $g_K(t) \propto \exp(-(t/\tau_K)^{\beta_K})$, where $\beta_K < 1$ and τ_K are fit parameters, seems adequate for describing the observed nonexponential decay of $C(t)$. KWW fits provided a good description in most cases, but failed for the 883-stars and for the two mixtures, which exhibit a more complex decay. An alternative choice is to fit data to a weighted sum of exponential functions. Excellent fits (lines in Figure 3) were obtained with five exponentials:

$$f(t) = \sum_{i=1}^{5} B_i \exp(-t/\tau_i), \tag{18}$$

Even if the fitting function provides a very good description of our data, the strong noise in the final decay of the correlation function makes the estimation of τ_a rather tricky. However, it is evident that the error bars in Figure 3 do not exceed the value $C(t) = 0.1$. We define the longest relaxation time of the short arm τ_a as the time at which the obtained fitting function drops to $C(\tau_a) = 0.1$. This value of $C(t)$ is rather small and at the same time, the noise at that level does not influence significantly the estimated value of τ_a. The average values of τ_a with corresponding errors for the simulated systems are listed in Table 2. In order to quantify the error of our estimation of τ_a, we fitted to Eq. (18) the 15 correlators computed for the different time origins. For each correlator we obtained a relaxation time from the condition $C(\tau_a) = 0.1$, and we calculated the standard deviation of the so-obtained 15 values of τ_a.

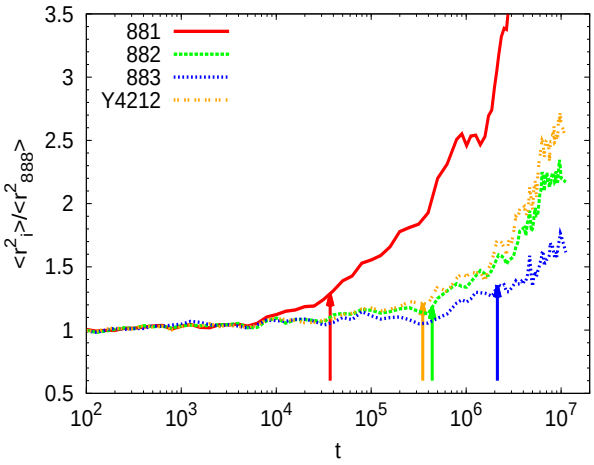

Figure 4: Ratio of the MSD of the T/Y-shaped asymmetric stars to the MSD of the reference symmetric stars as a function of time. The arrows are placed at the short arm relaxation times τ_a obtained by our method (see Table 2).

At this point it is worth studying the possible effect of the chosen method on the final value of p^2, namely by discussing other suggested approaches for obtaining τ_a from the simulation data. There have been some attempts to determine the longest relaxation time of the short arm, τ_a, from slip-link[28] and molecular dynamics simulations.[18] In the slip-link simulations τ_a was defined as the time when the short arm loses all its entanglements.[28] In the MD simulations[18] τ_a was determined as the time at which the MSD of the branchpoint of the asymmetric stars deviates from the corresponding data of the symmetric stars. This estimation is based on the assumption

that, after the short arm relaxation, the branchpoint is allowed to take a random hop along the confining tube. This change in the branchpoint dynamics leads to a change in the slope of the MSD. Zhou and Larson observed[18] that this change occurred at the time when the end-to-end correlation functions of the short arms decayed to $C(t) \approx 0.2$. However, there is no systematic method to find an accurate time, where the MSD curves for asymmetric and symmetric stars split up, so the values of τ_a estimated by the naked eye have a significant uncertainty (up to one time decade). Moreover, in order to obtain the τ_a for the mixtures we would need a reference system consisting of a mixture of symmetric stars and linear chains. In Figure 4 we show the results (arrows) obtained by our method (see above) together with MSD data of the branchpoint ($\langle r_{\mathrm{i}}^2 \rangle$) for different architectures. The latter are divided by the branchpoint MSD of the reference symmetric stars ($\langle r_{888}^2 \rangle$). In this representation, deviations from the branchpoint motion of the reference symmetric stars are reflected by deviations above the horizontal level $\langle r_{\mathrm{i}}^2 \rangle / \langle r_{888}^2 \rangle = 1$. By direct inspection of Figure 4 it seems that the precise point at which deviations arise is ill-defined (note the scatter in the data). Still, it is clear that the so-defined relaxation times are systematically smaller than those estimated by our method (arrows). As stated in Ref.,[18] the time at which the branchpoint MSD deviates from that of the reference symmetric stars is in very good agreement with the time at which the short arm correlation function decays to $C(t) = 0.2$. Obviously this corresponds to a shorter time scale that the relaxation time used by us, obtained as $C(\tau_a) = 0.1$ (see above). Namely, the former is about a 50 % smaller than our corresponding value for τ_a, which affects significantly the final value of p^2.

In the case of the mixtures of asymmetric stars and linear chains, p^2 is obtained from Eq. (12), which contains as additional parameter the relaxation time τ_s of the short linear chains in the mixture. We proceeded in a similar manner as for the short arms in the branched polymers, by analyzing the end-to-end correlator of the linear chains. However, the relaxation time of the linear chains is obtained in the usual way, as $C(\tau_s) = e^{-1}$, unlike the condition $C(\tau_a) = 0.1$ used for the *longest* relaxation time of the short arms. We find $\tau_s = 19000$.

4.3 Tube diameter and tube survival probability

As mentioned in the Introduction, one of the open questions regarding branchpoint dynamics is whether hopping takes place in the skinny (undilated) or in the fat (dilated) tube. In this subsection we investigate both cases and estimate from the simulation the corresponding values for the tube diameter. First we calculate the original skinny tube diameter, a_0, in our bead-spring polymers as:

$$a_0^2 = N_e^{PP} C_\infty b_0^2, \tag{19}$$

where C_∞ is the characteristic ratio, b_0 is the average bond length, and N_e^{PP} is the entanglement length estimated by primitive path analysis. We find $b_0 = 0.97$, and by analyzing the asymptotic behavior of intramolecular distances between distant beads (see Ref.[37] for details), we obtain $C_\infty b_0^2 = 3.46 \pm 0.10$ for all systems. We use the value $N_e^{PP} = 23$ reported by Everaers *et al.*,[35] which was obtained for a melt of bead-spring chains at the same density and temperature, and with identical interactions as those used in our work. By inserting the former values in Eq. (19), we obtain a diameter $a_0 = 8.92 \pm 0.13$ for the skinny tube.

In order to quantify the diameter of the fat tube for each investigated system, we first need to analyze the corresponding tube survival probability $\Phi(t)$.[38] The procedure for obtaining $\Phi(t)$ involves the calculation of the tangent correlation functions of polymer segments for the different investigated architectures. These provide information on the relaxation times of the primitive path coordinates, which can be used to determine the time dependence of the tube survival probability. A detailed description of the procedure is given in the Appendix. The obtained results for the tube survival probabilities are represented in Figure 5. The dilated tube diameter at the relaxation time τ_a of the short arm can be obtained as:[6,8]

$$a^2 = \frac{a_0^2}{\Phi^\alpha(\tau_a)} \tag{20}$$

where $\Phi(\tau_a)$ is the value of the tube survival probability at the average time τ_a (see above), and

α is the dilution exponent. In the analysis of the hopping parameter p^2 (see below) we will consider the two suggested values of the dilution exponent,[8] $\alpha = 1$ and $\alpha = 4/3$. As we discussed in the previous subsection, for each simulated system we use a set of 15 end-to-end correlators (computed at distinct time origins), yielding their respective values of τ_a. Accordingly, we have a corresponding set of 15 values for $\Phi(\tau_a)$. We use these for computing the standard deviations of $\Phi(\tau_a)$ (see below).

The calculated tube survival probability is directly related to the parameter ϕ^α in Eq. (11)-Eq. (12) via:

$$\phi^\alpha = \Phi^\alpha(\tau_a). \tag{21}$$

This parameter represents the fraction of the material that is responsible for the slow constraints in the system. After the relaxation of the fastest parts in our systems (short arms, and linear chains in the mixtures), the only slow components to relax are the long arms or main backbone. This information is contained in $\Phi(\tau_a)$, which measures the unrelaxed tube fraction at τ_a, i.e., at the time scale of the relaxation of the short arm. This is also the case for the investigated star/linear mixtures. Indeed the relaxation time for the linear chains is, at most, that of the short arms, since both have the same length (three entanglements, see Figure 1), but the short arms have only one free end.

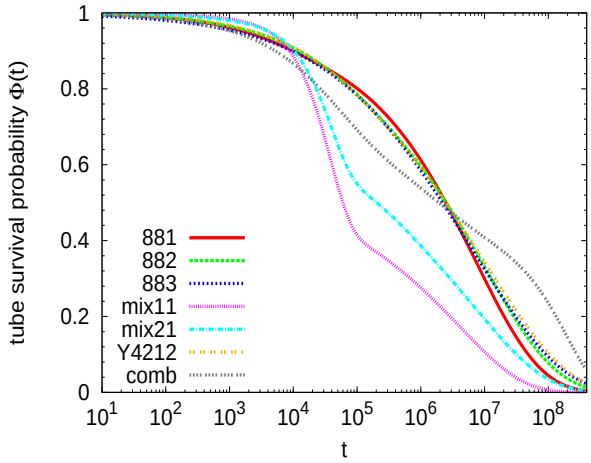

Figure 5: Tube survival probability obtained from the simulations (see Appendix) for all the investigated systems.

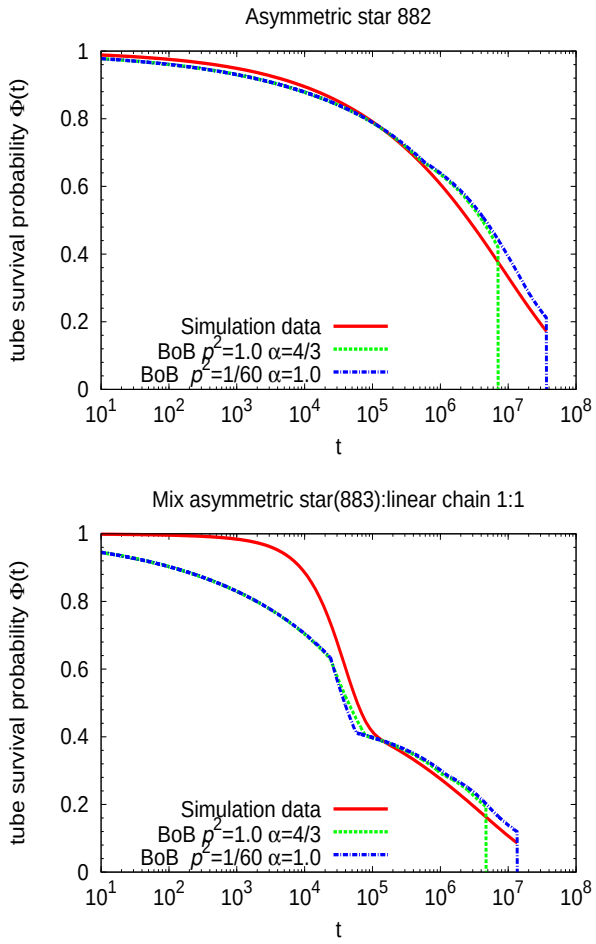

Figure 6: Comparison between the tube survival probabilities obtained from the simulations (solid line) and from the BoB model with choice of parameters $p^2 = 1, \alpha = 4/3$ (dashed line) and $p^2 = 1/60, \alpha = 1$ (dash-dot line).

Some general trends are inferred from simulation data in Figure 5. The two mixtures exhibit an abrupt decay in the range $10^4 \lesssim t \lesssim 10^5$. The beginning of this decay is consistent with the estimated relaxation time of the linear chains ($\tau_s = 19000$, see above). Thus, completion of the relaxation of the short linear chains leads to a sharp removal of constraints. As expected, the larger fraction of linear chains in the mixture 1:1 produces a stronger decay of $\Phi(t)$ than in the mixture 2:1. Differences in the tube survival probabilities of the T-shaped stars (881, 882, and 883) and the Y4212-stars are small at all time scales, which suggests a relatively small role of the relaxation of the short arms in the total $\Phi(t)$ of these systems, and once the short arms are relaxed, a similar amount of constraints are removed by reptation. The tube survival probability

of combs is markedly different from that of the T- and Y-stars. It shows a faster decay up to time scales of about τ_a. This is consistent with a stronger role of dynamic tube dilution in combs, due to their higher volume fraction of short arms than in the T- and Y-stars. However, after relaxation of the short arms, the combs contain two frictional fat beads close to the both ends of the linear backbone. This strongly hinders relaxation and $\Phi(t)$ exhibits a very slow decay over the following time decades, prior to the late decay by reptation.

The tube survival probabilities obtained from the simulations can be directly compared with theoretical predictions from hierarchical models. Here we compare our results with those from the branch-on-branch (BoB) model developed by Das *et al.* (see Ref.[3] for details). The BoB model makes detailed predictions for linear rheological data of non-looped branched architectures of arbitrary complexity, by using the entanglement length and entanglement time as external inputs. Output of the BoB calculation includes the tube survival probability $\Phi(t)$. Figure 6 compares BoB and simulation results of $\Phi(t)$ for some representative cases (882-stars and star/linear mixture 1:1). BoB assumes *a priori* values for α and p^2. The results in Figure 6 are obtained for two limit cases $p^2 = 1/60$, $\alpha = 1$ (dash-dot lines), and $p^2 = 1$, $\alpha = 4/3$ (dashed lines). These include the two values used for the scaling exponent α and the lowest and highest value of p^2 reported in the literature.[11] Both the hopping parameter p^2 and the scaling exponent (through the factor $\Phi^{-\alpha}(\tau_a)$) determine the friction constant for the final reptation of the system. Therefore, in systems where final relaxation is mediated by reptation, decreasing the values of p^2 and α moves the reptative regime to longer timescales. Thus, the cases $p^2 = 1/60$, $\alpha = 1$ and $p^2 = 1$, $\alpha = 4/3$ provide an upper and lower bound for the onset of reptation predicted by BoB. Relaxation by reptation in the BoB curves of Figure 6 corresponds to the final sharp drop to zero.[3] This time scale can change by even one decade according to the specific choice of p^2 and α.

Having noted this, the chosen values of p^2 and α do not significantly affect the obtained BoB curves in the time window, $t \leq \tau_a$ (relaxation before arm retraction is independent of p^2 and changing α from 1 to 4/3 introduces less than 0.1% difference in $\Phi(t)$ at τ_a for the molecules investigated), relevant for our estimations of p^2. Indeed, we estimate p^2 from the simulations by using

information on $\Phi(t)$ at the relaxation time of the short arms τ_a (through equations for the diffusivity in Section 3 and Eq. (21)), i.e., much *before* the onset of reptation. As shown in Figure 6 the two limit cases of p^2 and α used to generate the BoB curves lead to essentially the same results in the former time window, differences only arising at much longer times. Still, it must be noted that α should have a significant effect in that window for long side arms. In the cases investigated here the effect is negligible because the side arms are weakly entangled and stay in the early fluctuation regime.

In general, the simulation results for the tube survival probability are in qualitative agreement with the corresponding BoB results. The agreement is even semiquantitative in the case of the pure T-stars. The BoB model captures the trends observed by simulations, including the crossover between fast dynamics of the short linear chains/side branches and slow relaxation of the long backbone. Having said this, it must be noted that for some systems (Y4212-stars and combs) a significant part of the final relaxation of the backbone occurs at times beyond the simulation window ($t \gtrsim 4 \times 10^7$), so conclusions about the comparison at such time scales must be taken with care.

Once the reptation plateau in $\langle r^2 \rangle / t^{1/2}$, as well as τ_a and $\Phi(\tau_a)$ have been determined from the simulations, we can directly obtain the actual value of p^2 (see Section 6). According to the discussion in Section 3, different expressions will be used for p^2. These will depend on the specific architectures and compositions (pure or mixture), as well as on the choice of hopping in the dilated or in the skinny tube. In the different expressions of p^2, the values of τ_a and $\Phi(\tau_a)$ will enter separately and/or through the product $\tau_a \Phi^{2\alpha}(\tau_a)$ (see Section 6). Figure 7 shows simulation results of τ_a and the product $\tau_a \Phi^{2\alpha}(\tau_a)$, for the case of dilution exponent $\alpha = 4/3$, in comparison with the corresponding results obtained from the BoB model. A good agreement is again found, with some tendency for overestimation by BoB. Similar agreement is observed for the case $\alpha = 1$. With all this, we conclude that our procedure provides a robust estimation of tube survival probabilities and relaxation times of the short arms, allowing for a reliable estimation of the hopping parameter p^2, as will be discussed in Section 6.

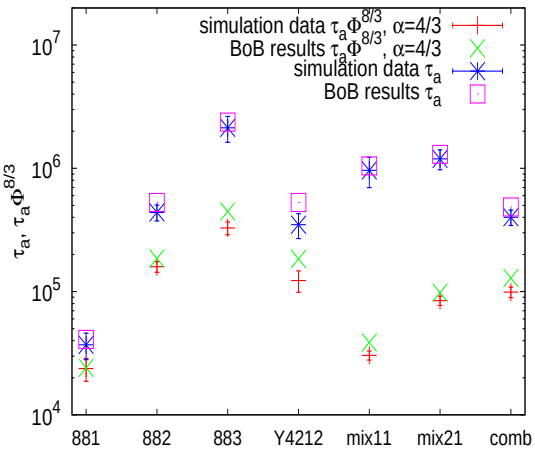

Figure 7: Comparison of the simulation results of τ_a and $\tau_a\Phi^{2\alpha}(\tau_a)$ with BoB predictions for the dilution exponent $\alpha = 4/3$.

4.4 Branchpoint trajectories

A further test of consistency for the estimated arm relaxation times can be obtained by analyzing the real-space trajectories of the branchpoints. Hierarchical models postulate branchpoint diffusion after relaxation of the short side arms. Prior to this, the branchpoint remains strongly localized. In order to test this hypothesis we have analyzed the shape of the trajectories at different time scales. Thus, for times $t > 10^5$ we have saved the coordinates of the branchpoint every $\tau = 2000$ time units. This roughly corresponds to one entanglement time ($\tau_e = 1800$). At earlier times we have used shorter intervals for saving the branchpoint positions. Namely we have used $\tau = 2 \times 10^{n-2}$ for the time decade $10^n < t \leq 10^{n+1}$, with $2 \leq n \leq 4$. With this, we use a large number of points (at least 50) to characterize the shape of the branchpoint trajectory at any relevant time. This characterization can be made by computing the asphericity parameter, defined as:

$$A = \frac{(I_2 - I_1)^2 + (I_3 - I_1)^2 + (I_3 - I_2)^2}{2(I_1 + I_2 + I_3)^2} \tag{22}$$

where I_1, I_2, I_3 are the semiaxes of the inertia ellipsoid of the trajectory. Thus, at each selected time t, we compute the asphericity $A(t)$ of the set of points consisting of the saved branchpoint positions at times $t' \leq t$. More precisely, for the time t we only use the points $t' \leq t$ saved every τ time units,

with τ the interval for saving used in the time decade which t belongs to (see above). For example, for $t = 4 \times 10^3$, we use the branchpoint positions at $t' \leq t$ saved every 20 time units. For any time $t > 10^5$ we use those saved every 2000 time units. In this way we get a fair characterization of the asphericity at any time, by always analyzing a set of points equispaced in time, and preventing 'crowding' in the regions visited by the branchpoint during the early time decades.

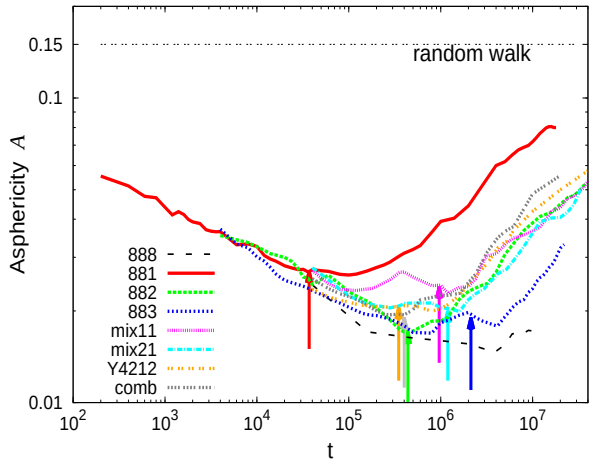

Figure 8: Time dependence of the asphericity of the branchpoint trajectory for all the simulated systems. The horizontal line represents the limit case of a random walk. The arrows indicate the relaxation times τ_a of the short arms, as determined independently from the analysis of their end-to-end correlators (see text).

Figure 8 shows the time dependence of the asphericity of the branchpoint trajectory for all the investigated systems. For comparison we include the value $A \approx 0.15$ obtained for a particle performing a three-dimensional random walk. The evolution of the asphericity with time reveals interesting features. In the early stage of the simulation, the asphericity diminishes by increasing time. This means that new positions of the branchpoint become localized in a limited region of the space, forming a trajectory that becomes closer and closer to the ideal spherical shape ($A = 0$). The asphericity reaches a minimum and then increases with time during the rest of the simulation, i.e., the branchpoint trajectory becomes progressively unlocalized. The random-walk limit is not reached at the end of the simulation. This will happen at much longer time scales, in the *three-dimensional isotropic* diffusive regime, $\langle r^2(t) \rangle \propto t$. Note that for the asymmetric systems, only one-dimensional curvilinear diffusion (reptation), $\langle r^2(t) \rangle \propto t^{1/2}$, has been reached within the simulation

window.

The minimum in the asphericity seems to follow several trends. For the three investigated T-shaped stars, it becomes deeper, i.e., the branchpoint becomes more localized, by increasing the length of the short arm. As expected, the strongest localization is found for the symmetric 888-stars. Localization in the 883-stars becomes weaker by mixing with short linear chains. In Figure 8 we have indicated (arrows) the relaxation times τ_a of the short arms, as obtained by the method presented in Section 4B. Within statistical error, there is a clear correlation between these time scales and the end of the localization of the branchpoint and later increase of the asphericity from the minimum. This result is consistent with the theoretical assumption of hopping of the branchpoint after full relaxation of the short arm.

5 Analysis: experiments

We use results from linear rheology measurements on a series of polystyrene (PS) and polyisoprene (PI) combs.[17,42] The mastercurves obtained from the dynamic frequency sweep measurements correspond to reference temperatures $T_{\rm ref} = 0^{\circ}$C for polyisoprene and $T_{\rm ref} = 170^{\circ}$C for polystyrene. Similarly to the simulation analysis, estimation of the arm relaxation time from comb experimental data presents some difficulties. In an effort to identify the arm relaxation time of the combs and to check the consistency of the obtained values we have used three different methods:

1. Analysis of the tube survival probabilities provided by the BoB computational algorithm. In this calculations we explicitly use the experimentally determined polydispersity indices in arm lengths (less than 1.1 in all cases).

2. Analysis of the intermediate peak in the frequency dependence of the experimental loss tangent $\tan\delta = G''(\omega)/G'(\omega)$.

3. Defining the time at which $G(t) = G_e\phi_{unr}^2$, where $G(t)$ and G_e are the experimental stress relaxation function and entanglement modulus, respectively. The quantity ϕ_{unr} is the fraction of unrelaxed material at the arm relaxation time (see below).

Table 1: Molecular characteristics[17,42,45] and parameters used in the estimation of τ_a of the experimental combs.

system	M_b (kg/mol)	M_a (kg/mol)	q	Z_{dil}	G_N (MPa)	M_e* (kg/mol)	M_e** (kg/mol)
PI254	120.5	18.8	7.1	11.4	0.41	5	4.09
PS642	275	47	29	2.9	0.22	16	13
PS732	860	25.7	26	30.3	0.22	16	13
PS742	860	47	29	20.8	0.22	16	13

*M_e was calculated from the plateau modulus G_N according to Ferry's definition, i.e., without the 4/5 prefactor.[43]

**M_e was calculated from the plateau modulus G_N according to the definition used in BoB and Fetters *et al.*,[44] i.e., with the 4/5 prefactor.

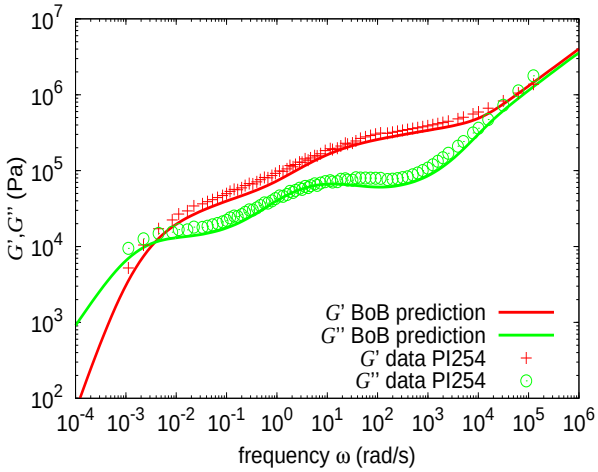

Figure 9: Linear rheology data of the PI254 combs.[42] Symbols: experimental data of $G'(\omega)$ and $G''(\omega)$ at reference temperature $T_{\mathrm{ref}} = 0°\mathrm{C}$. Lines: fits to the BoB model (see text for details).

The molecular characteristics of the combs are described in Table 1. All combs have a long well-entangled backbone (Z_b in the approximate range of 17 to 54 entanglements). The arms are weakly or moderately entangled (Z_a in the range of 1.6 to 6 entanglements). The values of Z_{dil} in Table 1 have been calculated by using Eq. (13) and entanglement molar masses M_e obtained from the Ferry's definition (column 7 in Table 1). The terminal relaxation times of the arms and backbone (see Table 5) differ by several orders of magnitude and therefore, it becomes possible to separate the two relaxation processes by using only linear rheology. The first method used to identify relaxation times includes the use of the BoB computational algorithm.[3] Figure 9 compares experimental data and BoB results for the PI254 comb at reference temperature $T_{\text{ref}} = 0°\text{C}$. The input parameters required by BoB are the entanglement molecular weight M_e, entanglement time τ_e, dilution exponent α and hopping parameter p^2. We set $\alpha = 1$ for all the studied systems. Good agreement with the experimental moduli is achieved by using $M_e(\text{PI}) = 4.09$ kg/mol and $\tau_e(\text{PI}) = 10^{-4}$ s at $T_{\text{ref}} = 0°\text{C}$. In the case of the PS combs we use $M_e(\text{PS}) = 13$ kg/mol and $\tau_e(\text{PS}) = 5 \times 10^{-4}$ s at $T_{\text{ref}} = 170°\text{C}$. The entanglement times τ_e chosen are shown to be consistent with previous works for the PS combs[17] and for the PI comb.[19,46] The plateau moduli corresponding to this set of parameters (listed in Table 1) are in agreement with published results of experimentally estimated G_N.[47] Whereas the PI microstructure is $\geq$90% 1,4-addition, even a small variation may slightly change the entanglement modulus G_e and τ_e. This may explain small variations in the values of these parameters in this and other works, but overall there is consistency. Architectural variability such as polydispersity in arms and backbone or uncertainty in the number and position of the branches is another possible source of discrepancy.[17] Although the TGIC (temperature gradient interaction chromatography) characterization on the PS combs confirmed their high level of purity ($>$ 85% target material),[42,48] the samples are still not perfect in terms of microstructural architecture. However, given the anticipated small effect,[24] further fractionation was not performed and this has not been further pursued in this work.

It must be noticed, that the molecular entanglement length defined in BoB is by a factor 4/5 smaller than the value of M_e used in our calculations (see Table 1). This difference follows from

the different definitions of M_e (see[43] for more details). The value of p^2 was selected to describe well the low frequency region of G' and G'' [1]. It is important to stress, as we discussed in Section 4.3, that the value of p^2 chosen for BoB prediction is irrelevant for further estimation of τ_a. Once we checked that BoB provides a good description of the linear rheological data we used additional output from BoB to estimate the arm relaxation time. Namely, by using the tube survival probability computed by BoB,[3] $\Phi(t)$, we obtain the arm relaxation time τ_a as the time for which $\Phi(\tau_a) = \phi_{unr}$, with ϕ_{unr} given by Eq. (23) below. Similarly to the work of Kapnistos *et al.*,[17] we include the contribution of the free backbone ends, and calculate the fraction of unrelaxed material after the full arm retraction as:

$$\phi_{unr} = 1 - (\phi_a + \phi_e) = 1 - \frac{qM_a + 2M_b/(q+1)}{qM_a + M_b}, \tag{23}$$

where ϕ_a and ϕ_e are the volume fraction of the arms and dangling backbone ends, respectively. The factor q is the number of side arms per comb. The quantities M_b and M_a are the molecular masses of the backbone and of each of the side arms, respectively. The values of all quantities included in Eq. (23) are given in Table 1.

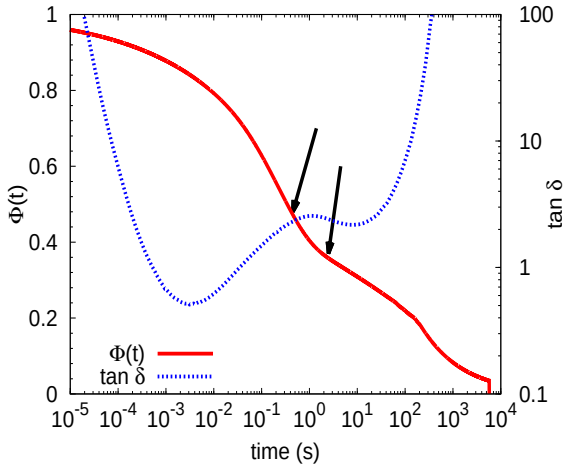

Figure 10: Unrelaxed volume fraction $\Phi(t)$ obtained from BoB (solid line) and experimental $\tan\delta$ (dashed line) versus time, for the PI254 comb. The arrows indicate the values of τ_a' and τ_a obtained by using $\Phi(\tau_a') = 1 - \phi_a$ and $\Phi(\tau_a) = 1 - (\phi_a + \phi_e)$, respectively.

[1] $p^2 = 1/40$ for PI254, p^2 equal to $1/10$ in case of PS642 combs, $p^2 = 1/12$ was set for PS732 and PS742 samples

We have also determined the time τ_a' at which the fraction of unrelaxed material is given by $\Phi(\tau_a') = 1 - \phi_a$. This gives us a lower bound for the estimation of the arm relaxation time. Figure 10 shows the time dependence of the function $\Phi(t)$ obtained by the BoB model for the case of PI254. We indicate (arrows) the times τ_a' and τ_a, obtained from the BoB model as explained above. For comparison, we plot in the same figure the experimental loss tangent versus inverse frequency. The intermediate peak in $\tan\delta$ falls in between the two relaxation times τ_a' and τ_a. From the plot of unrelaxed fraction versus time we can identify two main relaxation processes. The final relaxation time of the arms is at the transition point between these two processes. We find the same qualitative behavior than in the $\Phi(t)$ of the simulated combs (Figure 5), with a very slow decay after τ_a extending over several decades prior to the final reptational decay.

In the second method we determine τ_a by analyzing the intermediate peak in the frequency representation of the experimental $\tan\delta$. The first step is to fit the curves with, e.g., a Gaussian or a Lorentzian function. One example of the fitting procedure is shown in Figure 11. Then we estimate τ_a as the inverse of the peak of the so-obtained fitting function. Another estimation can be obtained from the derivative of the experimental $\tan\delta$-curve, by defining τ_a as the inverse frequency at the point in which the derivative becomes zero.

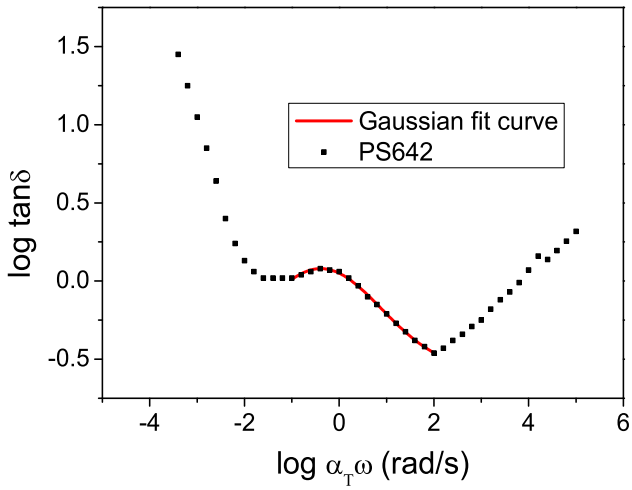

Figure 11: Symbols: frequency dependence of $\tan\delta$ for the PS642 comb (log-log representation). The line is a Gaussian fit of the peak. α_T is the horizontal shift factor, for the presented data ($T = 170^\circ$C) α_T is equal to 1.

Finally, we make another estimation of the arm relaxation time by analyzing the experimental stress relaxation modulus $G(t)$. The tube model in combination with the dynamic dilution theory[41] provides an expression for the relaxation modulus $G(t)$ consisting of two contributions: (i) fast Rouse modes together with longitudinal Rouse modes in the tube that represent 1/5 of the G_e relaxation, (ii) escape from the tube at longer times related to the plateau modulus $G_N = \frac{4}{5}G_e$. One may generally assume that, at the times comparable to the relaxation time of the side arms, the first contribution has already relaxed. However, in the comb architecture where the longitudinal modes are primarily operative at the backbone, this relaxation mechanism may depend on the number and position of branchpoints on the backbone. In all experimental combs used for this analysis the average distances between the branchpoints are very small, in most cases $Z_{dil}/q \ll 1$. Therefore the relaxation modes involving the motion of the backbone along the tube are frozen during the relaxation of the side arms. Only small fluctuations of the backbone between consecutive branchpoints are present. Following this argument and assuming a dilution exponent $\alpha = 1$,[17,19,24] at the end of the arm relaxation the relaxation modulus will be $G(\tau_a) = G_e\phi_{unr}^2$ instead of the value $G(\tau_a) = G_N\phi_{unr}^2$ expected for $Z_{dil}/q > 1$. We would like to draw attention to this issue, because the suppression of the longitudinal Rouse motion seems to be a general feature of densely grafted combs. We use in the calculation an entanglement modulus $G_e = \frac{5}{4}G_N = 5.1 \times 10^5$ Pa for PI and $G_e = 2.8 \times 10^5$ Pa for PS. These values are consistent with the above reported values of M_e, in the sense that they obey rubber elasticity[49] within 15% at reference temperatures given above. Figure 12 shows experimental results for the relaxation modulus in the different investigated systems. We indicate by arrows the corresponding values of τ_a estimated by this method.

By combining the results obtained by the different methods presented in this section, we determine an upper and lower bound for the arm relaxation time τ_a in each of the investigated comb polymers. These values are given in Table 5.

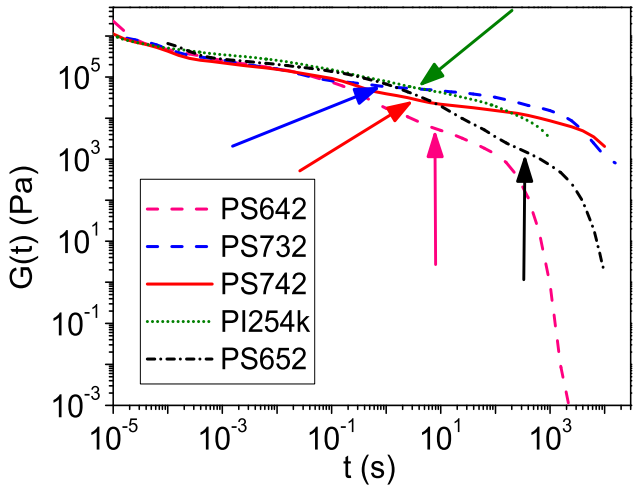

Figure 12: Experimental stress relaxation modulus for the investigated comb polymers. The arrows indicate the arm relaxation times estimated from the relation $G(\tau_a) = G_e \phi_{unr}^2$ (see text).

Table 2: Summary of the variables obtained from the simulations: reptation plateau in MSD ($\langle r^2 \rangle / t^{1/2} \sim t^0$), longest relaxation time of the short arm (τ_a), and tube survival probability at the time τ_a ($\Phi(\tau_a)$).

system	$\langle r^2 \rangle / t^{1/2}$	τ_a	$\Phi(\tau_a)$
881	0.066±0.003	37000±9000	0.849±0.011
882	0.031±0.001	439000±65000	0.685±0.013
883	0.023±0.001	2133000±507000	0.500±0.023
Y4212	0.036±0.001	349000±80000	0.678±0.009
mix11	0.064±0.004	962000±265000	0.278±0.021
mix21	0.045±0.002	1193000±221000	0.373±0.014
comb	0.036±0.002	401000±57000	0.593±0.010

6 Hopping parameter: Results and discussion

Now we use the information obtained from the analysis in Section 4 and Section 5, as input for obtaining the numerical values of p^2 for each of the investigated systems. The values of the observables estimated from simulations — reptation plateau in MSD ($\langle r^2\rangle/t^{1/2} \sim t^0$) longest relaxation time of the short arm (τ_a), and tube survival probability at the time τ_a ($\Phi(\tau_a)$) — are summarized in Table 2. By inserting these values, together with the tube diameter, into the equations presented in Section 3, we can calculate the hopping parameter p^2. If the backbone friction is not considered, by combining Eq. (9) and Eq. (10) for the diffusivity we obtain:

$$p^2 = \frac{q\pi\tau_a}{2a_h^4}\left(\frac{\langle r^2\rangle}{t^{1/2}}\right)^2. \tag{24}$$

In this equation we use $a_h^4 = a_0^4$ if hopping is assumed to occur in the skinny undilated tube. In the case of hopping in the dilated tube, according to Eq. (20) we use $a_h^4 = a_0^4/\Phi^{2\alpha}(\tau_a)$.

If we consider the backbone friction, then we make use of Eq. (11) for the pure branched systems and Eq. (12) for the star/linear mixtures. By combining each of these cases with Eq. (9) we obtain the general expression for the hopping parameter:

$$p^2 = \frac{2qa_0^4\pi\tau_a}{a_h^4}\left[\frac{(\langle r^2\rangle/t^{1/2})^2}{4a_0^4 - 3\pi^3\tau_e ZQ(\langle r^2\rangle/t^{1/2})^2}\right]. \tag{25}$$

Again, $a_h^4 = a_0^4$ or $a_h^4 = a_0^4/\Phi^{2\alpha}(\tau_a)$ if hopping takes place in the skinny or dilated tube, respectively. The number of entanglements along the backbone is $Z = 16$ for all the simulated systems (see Figure 1). The number of side arms is $q = 1$ in star-like structures and $q = 2$ in the case of combs. The factor Q is equal to 1 in the case of the pure systems, whereas for the mixtures it stands for:

$$Q = \Phi^\alpha \frac{2\tau_s(1-\Phi^\alpha) + 3\pi^2 c_\nu \tau_e}{2\tau_s\Phi^\alpha(1-\Phi^\alpha) + 3\pi^2 c_\nu \tau_e}. \tag{26}$$

We assume a constraint-release rate constant[39] $c_\nu = 0.1$ in the two investigated mixtures of T-stars and short linear chains.

The reciprocal values of the hopping parameter $1/p^2$ for the simulated systems, calculated by using Eq. (24) (no backbone friction) and Eq. (25) (including backbone friction) are summarized in Table 3 and Table 4 respectively, for both dilution exponents $\alpha = 1$ and $4/3$. In both Tables we just give the minimum and maximum possible values of p^2 in each system. For getting these values, we have made the corresponding combinations of the upper and lower values (given by their respective error bars, see Section 4) of the parameters entering in the former equations for p^2, and have selected the minimum and maximum output of such equations. This allows us to estimate p^2 within an uncertainty of typically about a factor 2.

Table 3: Results of the calculation of $1/p^2$ in the simulated systems without considering additional friction of the backbone (i.e., by using Eq. (24)). Underlined data are further compared to experimental results (Figure 14). First column: simulated systems. Second to fourth columns: values of $1/p^2$. In the first two lines we indicate the used values of the dilution exponent ($\alpha = 1$ or 4/3), and whether hopping occurs in the skinny tube ($a_h = a_0$) or in the dilated one ($a_h = a$).

α	1	4/3	1	4/3
$1/p^2$	$a_h = a_0$	$a_h = a_0$	$a_h = a$	$a_h = a$
881	17-38	17-38	25-51	28-56
882	7-13	7-13	16-27	21-35
883	3-5	3-5	11-20	18-30
Y4212	6-13	6-13	14-28	19-36
mix11	1-2	1-2	10-19	25-42
mix21	1-2	1-2	9-16	19-31
comb	3-5	3-5	<u>9-15</u>	12-20

Table 4: As in Table 3, but considering the additional friction of the backbone (i.e., by using Eq. (25)).

α	1	4/3	1	4/3
$1/p^2$	$a_h = a_0$	$a_h = a_0$	$a_h = a$	$a_h = a$
881	8-23	8-23	11-30	13-34
882	7-12	7-12	14-25	19-32
883	2-5	2-5	11-19	17-29
Y4212	5-12	5-12	12-25	16-32
mix11	1-2	1-2	9-18	25-41
mix21	1-2	1-2	9-16	18-30
comb	2-5	2-5	<u>7-13</u>	10-18

The values of $1/p^2$ calculated from the simulation results are plotted in Figure 13. There is

a big gap between the values obtained by assuming hopping in the skinny or in the dilated tube. The gap in the $1/p^2$-values is indeed proportional to the factor $1/\Phi^{2\alpha}(\tau_a)$ arising from assuming $a_h^4 = a_0^4$ or $a_h^4 = a_0^4/\Phi^{2\alpha}(\tau_a)$ in Eq. (24) and Eq. (25). The effect of the tube widening on the former gap is, therefore, more pronounced in the systems where a significant part of the molecule has been relaxed at the time τ_a. One clear example is the mixture 1:1. In this system, and for dilution exponent $\alpha = 1$, the value of $1/p^2$ for hopping in the dilated tube is about 10 times bigger than the corresponding value for hopping in the skinny tube.

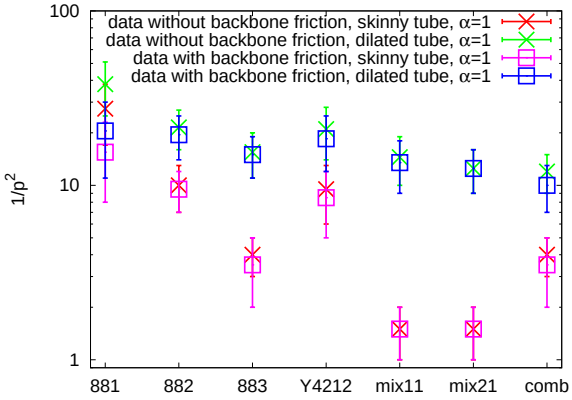

Figure 13: Representation of the results of Table 3 and Table 4 for $\alpha = 1$. Symbols are the averages of the respective upper and lower values of $1/p^2$.

The question of the apparent high friction exerted by the slightly entangled short arms seems to be rationalized if one accounts for the effect of the backbone friction on the branchpoint diffusivity. This effect is nicely illustrated in the case of the 881-stars, where the short arm is only one entanglement long, and therefore the contribution of the backbone friction is expected to play a relevant role in the diffusion of the branchpoint along the tube. For the case of $\alpha = 1$ and hopping in the dilated tube, the value of $1/p^2$ for the 881-stars without including the backbone friction is about 40. If we include the backbone friction in the diffusion constant the value of $1/p^2$ is lowered to approximately 20, which is much closer to the respective values obtained for the other systems.

We now restate our criterion, presented in the Introduction, for what constitutes a good set of assumptions about branch-point hopping: a good set of assumptions should result in broadly similar values of p^2 across the different systems studied. By inspection of Table 3 and Table 4

and Figure 13, we conclude that a comparatively low dispersion in the values of $1/p^2$ is found *only* if the backbone friction is included in the diffusivity and hopping is assumed to occur in the dilated tube. This set of assumptions leads to roughly a factor 2 variation in the value of $1/p^2$ across the systems studied, which is within the error bounds of our analysis. As is emphasized by the logarithmic axis in Figure 13, results for other combinations of specific assumptions for branchpoint hopping are very disperse, suggesting that they are inconsistent and can be ruled out in models. For example, setting the length scale associated with the hops to the bare (skinny) tube diameter leads to a very wide range of the p^2 values for different branched structures (variation by a factor of 10, which is significantly beyond the error bounds of our analysis).

With the assumptions of both inclusion of backbone friction and hopping in the dilated tube, the mean values of $1/p^2$ (defined for each system as the mean of the upper and lower bound) fluctuate between 10 and 20.5 if we use the dilution exponent $\alpha = 1$, and between 14 and 33 if we use $\alpha = 4/3$. Thus, the diffusion of the branch point in the dilated tube with incorporated backbone friction points to an universal behavior described in many experimental studies with parameter $1/p^2 = 12$.[12,13,19]

Now we discuss results for the experimental combs. The corresponding expression for the hopping parameter p^2 can be obtained, by combining Eq. (10), Eq. (13), Eq. (14) and Eq. (15), as:

$$p^2 = \frac{2\tau_a q Z_{dil}^2}{\pi^2 \tau_d}\left(1 - \frac{3.38}{Z_{dil}^{1/2}} + \frac{4.17}{Z_{dil}} - \frac{1.55}{Z_{dil}^{3/2}}\right). \tag{27}$$

By using in Eq. (27) the upper and lower bounds of τ_a and τ_d we determine the minimum and maximum possible values of the hopping parameter. See Table 5 for the values of the quantities in Eq. (27) (Z_{dil} is calculated from Eq. (13) and is placed in Table 1). The terminal time τ_d was calculated as the product of the zero-shear viscosity η_0 and the zero-shear recoverable compliance J_0.[49] The expression for τ_d reads:

$$\tau_d = \eta_0 J_0 = \eta_0 \frac{1}{\eta_0^2} \lim_{\omega\to 0} \frac{G'}{\omega^2} = \frac{\lim_{\omega\to 0}(G'/\omega^2)}{\lim_{\omega\to 0}(G''/\omega)}. \tag{28}$$

Both zero-shear limits of the linear rheology data were approximated by fitting to the empirical Carreau and Cross models.[50] Then the lower and upper bounds of the obtained limits were combined in order to get the range of τ_d values (see Table 5). This method of determination of the relaxation time is more prone to error when the terminal relaxation ($G' \sim \omega^2$ and $G'' \sim \omega$) has not yet been attained as is the case of the comb PS742. In the case of this comb, the uncertainty in the terminal time is much higher than in the other combs. The relaxation times τ_d determined from Eq. (28) are larger than the relaxation times estimated from the crossover of G' and G'' to terminal relaxation.[48] This is expected for combs with entangled branches since there is an additional mode of relaxation in the terminal regime. More details about the determination of τ_d can be found in.[48]

Table 5: Summary of relaxation times and hopping parameters obtained for the experimental combs. The particular method used for the estimation of τ_a is written in square brackets.

system	τ_d (s)	τ_a [BoB] (s)	τ_a [tanδ] (s)	τ_a [$G(t)$] (s)	$1/p^2$
PI254	580-730	0.4-2.5	0.9-1.2	1.9	4-30
PS642	84-93	1.7-1.9	2.2-2.5	5.3	5-8
PS732	3200-3900	0.07-0.11	0.04-0.05	0.16	8-39
PS742	7700-13000	0.8-1	0.7-0.9	1.3	5-16

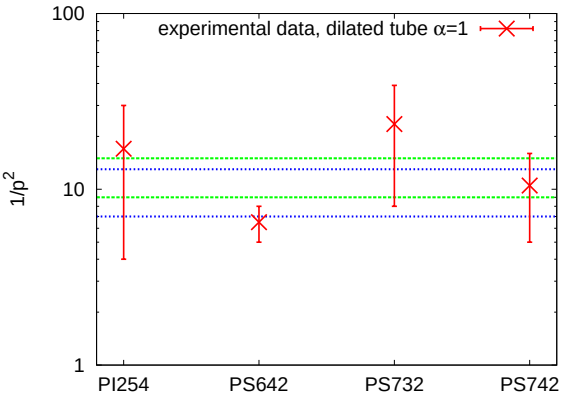

Figure 14: Hopping parameters for the combs. Symbols are the averages of the respective upper and lower values of $1/p^2$ for the experimental combs. Green lines indicate the lower and upper value obtained from the simulation data, without considering the backbone friction (underlined data in Table 3). Blue lines represent the analogous results if backbone friction is considered (underlined data in Table 4).

In Figure 14 we compare the estimated values for $1/p^2$ in the five experimental comb polymer melts with the results in the simulated comb. For the latter we include the upper and lower limits, for the case of $\alpha = 1$ and hopping in the dilated tube, without considering backbone friction (underlined data in Table 3) and considering backbone friction (underlined data in Table 4). The experimental data lay close or within the bounds given by the simulation values. The only exception is the PS732 sample. It must be noted that, except for the relaxation times τ_a and τ_d, the numerical values of the quantities entering in Eq. (27) are known with high accuracy. The strong discrepancy between the $1/p^2$ value obtained for the PS732 comb and the values obtained for the other combs might originate from a poor estimation of its τ_a. By comparing the τ_a and p^2 values obtained from different methods we found that the highest value of $1/p^2$ in case of the PS732 arises from the tangent loss peak analysis. This analysis is based on the assumption that the two relaxation processes of the short side branches and the backbone are *independent and well-separated*. If this assumption is not fulfilled, the $\tan\delta$-peak will contain more contributions than the simple arm relaxation, what will bias the analysis. This seems plausible since the side branches in the PS732 comb are weakly entangled ($Z_a \sim 2$). Incidentally, same issues may arise if the branches are too long and effectively dilute the backbone too much. This is the case when the arm and backbone relaxation times are too close.[17,51] Hence, the precise determination of the arm relaxation time of the combs remains a subtle issue and cannot be accomplished without combining experiments and modeling. Regarding the PS642 combs, it must be noted that the dilution of the backbone is beyond the limits captured by the models ($Z_{dil} = 2.9$). Nevertheless, by assuming, even in this limiting case, that after the relaxation of the side arms the branched polymer is reduced to an effective linear chain described by the Likhtman-McLeish theory,[41] the values of the hopping parameter obtained from the analysis of the linear rheology data are comparable to those found in the simulations.

7 Conclusions

We have performed large-scale molecular dynamics simulations of melts of entangled branched polymers: symmetric stars, asymmetric T-shaped and Y-shaped stars, combs and mixtures of stars and linear chains. An analysis of the branchpoint trajectories reveals that delocalization of the branchpoint begins at the relaxation time of the respective side arm. The results for the mean squared displacement, at times far beyond the relaxation time of the short side arms, are consistent with reptation of the diluted linear backbone. Both observations are in qualitative agreement with assumptions invoked in hierarchical tube models for branched polymers.

We have analyzed the diffusive motion and friction of the branchpoints, as well as dynamic tube dilution, by using direct information from the simulation data. We have determined the values of the hopping parameter, p^2, for each set of specific assumptions made by hierarchical models for branchpoint hopping. Including the contribution from the backbone friction, and considering hopping in the dilated tube, provides the only consistent set of hopping parameters in the different architectures, with $1/p^2$ found to be in the range $10-20$ for dilution exponent $\alpha = 1$, and in the range $14-33$ for $\alpha = 4/3$. Other combinations of specific assumptions for branchpoint hopping lead to disperse, inconsistent sets of p^2-values, suggesting that they can be ruled out in the implementation of hierarchical tube models. The analysis of linear rheological data for comb polymers confirm the findings obtained from simulations.

8 Acknowledgements

This work has been supported by the projects FP7-PEOPLE-2007-1-1-ITN (DYNACOP, Marie Curie Network, European Union), MAT2012-31088 (Spain) and IT654-13 (GV, Spain). We acknowledge the programs PRACE, HPC-Europa2 and ESMI (European Union), and ICTS (Spain) for generous allocation of CPU time at GENCI (Paris, France), HLRS (Stuttgart, Germany), FZJ-JSC (Jülich, Germany), and CESGA (Santiago de Compostela, Spain).

A Calculation of the tube survival probability

As first proposed by Doi and Edwards, and examined in the simulation work of Stephanou *et al.*,[52] the tube survival probability can be obtained from the tangent correlation function. This function can be expressed as:

$$\phi_\ell(t) = \langle \mathbf{u}_{\alpha,\ell,0} \cdot (\mathbf{R}^e_{\alpha,t} + B'\mathbf{R}^e_{\beta,t} + C'\mathbf{R}^e_{\gamma,t}) \rangle. \tag{29}$$

The indices $\alpha, \beta, \gamma \in \{1,2,3\}$ label the three arms in the case of the star (T- and Y-) architecture, and the two short arms and half of the backbone in the case of the comb. For simplicity, in the following we will also refer to the half-backbone in the comb as 'arm'. The vector $\mathbf{R}^e_{\alpha,t}$ is the end-to-end vector of the particular arm α at time t. The tangent vector $\mathbf{u}_{\alpha,\ell,0} = \partial \mathbf{r}_{\alpha,\ell,0}/\partial \ell$, at the ℓth segment of the arm α at time 0, is approximated in the simulation analysis by the end-to-end vector of the ℓth segment (see below). The numerical coefficients B' and C' express the weight of the correlation between the parts α, β and γ of the molecule. We consider three possible values of the coefficients: 0 (no correlation), -1 (full correlation) or -1/2 (half correlation). In our previous work, we confronted our choice of the coefficients with the predictions of the Rouse model.[38] It turned out that, in the case of the 3-arm *symmetric* stars two neighboring arms contribute equally with a prefactor -1/2 to the correlation with the third arm. The introduction of the full correlation ($B' = C' = -1$) led to artificial peaks in the correlation function of the segments close to the branch point. Following this argument, in this work we use $B' = C' = -1/2$ for the case of the Y-shaped stars. However, the situation is a bit different in the case of T-shaped stars, where there are two equally long arms and one short arm. The tangent correlator of each of the long arms is largely dominated by correlations with the segments of both long arms. Hence, we can omit the correlations with the short arm in the tangent correlators of the long arms, taking the corresponding coefficient as zero. We treat the linear chains in the star/linear mixtures as 2-arm stars, and we use the same coefficients as in the case of the T-shaped stars (Figure 15a). In the case of the comb we use a similar procedure based on the decomposition of the molecule into symmetric and asymmetric regions. Figure 15 shows an schematic representation of all the correlations and

corresponding coefficients for the T-shaped stars and comb.

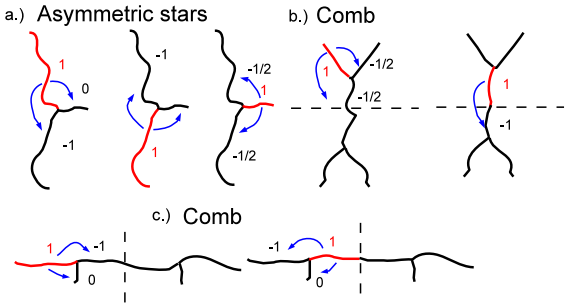

Figure 15: Schematic representation of the weight of the correlations used for the tangent correlator: a) T-stars, b) and c) comb. Numbers labelling particular segments are the prefactors used in Eq. (29). The part α containing the ℓth segment in this equation is represented with red color.

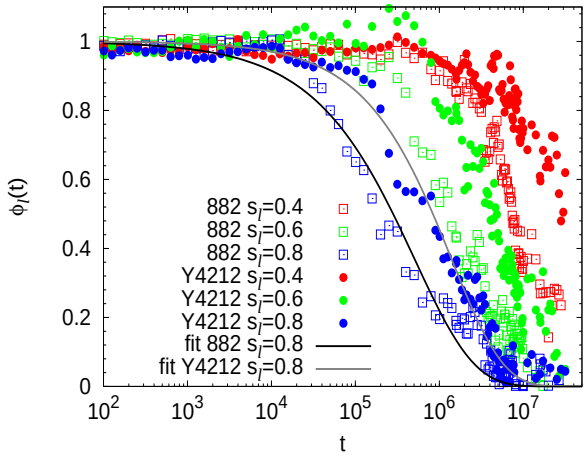

Figure 16: Symbols: tangent correlation functions of three segments $s_\ell = 0.4$ (red), $s_\ell = 0.6$ (green) and $s_\ell = 0.8$ (blue) in the long arms of the 882 T-shaped (squares) and Y-shaped Y4212 (circles) asymmetric stars. Lines are two representative KWW fits.

We calculate the tangent correlation function according to Eq. (29), where we define $\mathbf{u}_{\alpha,\ell,0}$ as the end-to-end vector of finite segment ℓ. We use segments of length of ten beads, which constitutes a good compromise. The choice of longer or shorter segments does not change the character of the correlation function, but the so-obtained function lacks of good statistics or is biased by fast monomer fluctuations (not captured in the original tube survival probability). Figure 16 shows the functions $\phi_\ell(t)$ of three selected segments in the 882 T-shaped stars and Y4212 Y-shaped stars. In both cases the selected segments are placed in the long arms. The segmental tangent correlation

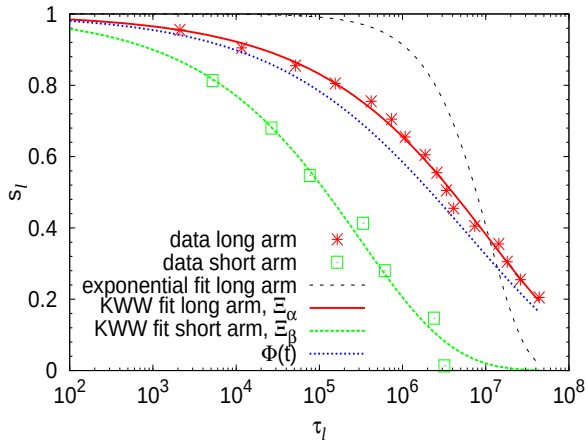

Figure 17: Illustration of the procedure for obtaining the tube survival probability in the 883-star. The data $[s_\ell; \tau_\ell]$ for the long (red symbols) and short (green symbols) arms are fitted to KWW functions. The dashed line represents a single exponential function. The final tube survival probability, calculated according to Eq. (31), is given by the blue line.

functions were fitted to a KWW function (Figure 16),

$$\phi_\ell(t) = \exp(-(t/\tau_\ell)^\beta) \tag{30}$$

where τ_ℓ and β are fit parameters. The spectrum of the relaxation times τ_ℓ of all the ℓth-segments provides us the information about the progressive relaxation of the molecule. We use the set of points $[s_\ell; \tau_\ell]$ to construct the tube survival probability $\Phi(t)$. By counting $\ell = 1$ to $\ell = \ell_{max}$ from the branch point to the outermost segment, the 'path cordinate' is defined as $s_\ell = \ell/\ell_{max}$.

The procedure to construct the tube survival probability $\Phi(t)$ is illustrated in Figure 17 for the T-shaped 883-stars. The discrete set of data $[s_\ell, \tau_\ell]$ for each arm can be described by an empirical function, which allows us to assign, in a continuous way, a fraction of unrelaxed arm to every time t. It is evident from Figure 17 that the time evolution of this fraction does not follow a single exponential decay (dashed line). Instead, a KWW function (red and green lines) provides an excellent description of the data. We use the so-obtained KWW functions to construct the smooth, continuous functions $\Xi_{\alpha,\beta,\gamma}(t)$ corresponding to the tube survival probability of each arm α,β,γ. The function starts at $\Xi_{\alpha,\beta,\gamma}(0) = 1$ (when the whole arm is unrelaxed), and decays to zero,

$\Xi_{\alpha,\beta,\gamma}(\tau_a) = 0$, at the longest relaxation time of the arm. In the case of the T-shaped asymmetric stars the tube survival probabilities of the two long arms are identical (only one of both is shown in Figure 17). There is a straightforward relation between the obtained partial functions $\Xi_{\alpha,\beta,\gamma}(t)$ and the final tube survival probability:

$$\Phi(t) = \frac{Z_\alpha \Xi_\alpha(t) + Z_\beta \Xi_\beta(t) + Z_\gamma \Xi_\gamma(t)}{Z_\alpha + Z_\beta + Z_\gamma}. \tag{31}$$

In this equation $Z_{\alpha,\beta,\gamma}$ stands for the number of entanglements of the distinct arms α, β and γ respectively. In the star/linear mixtures (mix21, mix11) we have to add the tube survival probability of the linear chains with the appropriate weight. Thus, the final tube survival probability of the 2:1 mixture is $\Phi(t) = (2\Phi_{883} + \Phi_{lin})/3$, and in case of the 1:1 mixture it is equal to $\Phi(t) = (\Phi_{883} + \Phi_{lin})/2$, where the functions Φ_{883} and Φ_{lin} are obtained separately by using Eq. (31) with their respective values of $Z_{\alpha,\beta,\gamma}$ and $\Xi_{\alpha,\beta,\gamma}(t)$. The tube survival probabilities of all the simulated systems, calculated according to Eq. (31), are shown in Section 4.3 of the manuscript (Figure 5).

References

(1) Read, D. J.; Auhl, D.; Das, C.; den Doelder, J.; Kapnistos, M.; Vittorias, I.; McLeish, T. C. B. *Science* **2011**, *333*, 1871–1874.

(2) Larson, R. G. *Macromolecules* **2001**, *34*, 4556–4571.

(3) Das, C.; Inkson, N. J.; Read, D. J.; Kelmanson, M. A.; McLeish, T. C. B. *Journal of Rheology* **2006**, *50*, 207–234.

(4) van Ruymbeke, E.; Bailly, C.; Keunings, R.; Vlassopoulos, D. *Macromolecules* **2006**, *39*, 6248–6259.

(5) Doi, M.; Edwards, S. F. *The Theory of Polymer Dynamics*; Oxford University Press, USA, 1986.

(6) McLeish, T. C. B. *Advances in Physics* **2002**, *51*, 1379–1527.

(7) Dealy, J. M.; Larson, R. G. *Structure and Rheology of Molten Polymers - From Structure to Flow Behavior and Back Again.*; Hanser Publishers, 2006.

(8) Milner, S. T.; McLeish, T. C. B. *Macromolecules* **1997**, *30*, 2159–2166.

(9) Marrucci, G. *Journal of Polymer Science: Polymer Physics Edition* **1985**, *23*, 159–177.

(10) McLeish, T. C. B. *Journal of Rheology* **2003**, *47*, 177–198.

(11) Frischknecht, A. L.; Milner, S. T.; Pryke, A.; Young, R. N.; Hawkins, R.; McLeish, T. C. B. *Macromolecules* **2002**, *35*, 4801–4820.

(12) Chen, X.; Larson, R. G. *Macromolecules* **2008**, *41*, 6871–6872.

(13) McLeish, T. C. B. et al. *Macromolecules* **1999**, *32*, 6734–6758.

(14) As noted in Ref.,[15] a value $p^2 = 1/6$ was erroneously reported in the original article.

(15) Daniels, D. R.; McLeish, T. C. B.; Crosby, B. J.; Young, R. N.; Fernyhough, C. M. *Macromolecules* **2001**, *34*, 7025–7033.

(16) Inkson, N. J.; Graham, R. S.; McLeish, T. C. B.; Groves, D. J.; Fernyhough, C. M. *Macromolecules* **2006**, *39*, 4217–4227.

(17) Kapnistos, M.; Vlassopoulos, D.; Roovers, J.; Leal, L. G. *Macromolecules* **2005**, *38*, 7852–7862.

(18) Zhou, Q.; Larson, R. G. *Macromolecules* **2007**, *40*, 3443–3449.

(19) Kirkwood, K. M.; Leal, L. G.; Vlassopoulos, D.; Driva, P.; Hadjichristidis, N. *Macromolecules* **2009**, *42*, 9592–9608.

(20) Lee, J. H.; Fetters, L. J.; Archer, L. A. *Macromolecules* **2005**, *38*, 10763–10771.

(21) Tezel, A. K.; Leal, L. G. *Macromolecules* **2006**, *39*, 4605–4614.

(22) Zamponi, M.; Pyckhout-Hintzen, W.; Wischnewski, A.; Monkenbusch, M.; Willner, L.; Kali, G.; Richter, D. *Macromolecules* **2010**, *43*, 518–524.

(23) Ahmadi, M.; Bailly, C.; Keunings, R.; Nekoomanesh, M.; Arabi, H.; van Ruymbeke, E. *Macromolecules* **2011**, *44*, 647–659.

(24) Snijkers, F.; van Ruymbeke, E.; Kim, P.; Lee, H.; Nikopoulou, A.; Chang, T.; Hadjichristidis, N.; Pathak, J.; Vlassopoulos, D. *Macromolecules* **2011**, *44*, 8631–8643.

(25) Chen, X.; Lee, H.; Rahman, M. S.; Chang, T.; Mays, J.; Larson, R. *Macromolecules* **2012**, *45*, 5744–5756.

(26) Chen, X.; Rahman, M. S.; Lee, H.; Mays, J.; Chang, T.; Larson, R. *Macromolecules* **2011**, *44*, 7799–7809.

(27) Lee, J. H.; Fetters, L. J.; Archer, L. A. *Macromolecules* **2005**, *38*, 4484–4494.

(28) Shanbhag, S.; Larson, R. G. *Macromolecules* **2004**, *37*, 8160–8166.

(29) Masubuchi, Y.; Yaoita, T.; Matsumiya, Y.; Watanabe, H. *The Journal of Chemical Physics* **2011**, *134*, 194905.

(30) Archer, L. A.; Juliani, *Macromolecules* **2004**, *37*, 1076–1088.

(31) Park, S.; Shanbhag, S.; Larson, R. *Rheologica Acta* **2005**, *44*, 319–330.

(32) Wang, Z.; Chen, X.; Larson, R. G. *Journal of Rheology* **2010**, *54*, 223–260.

(33) Kremer, K.; Grest, G. S. *The Journal of Chemical Physics* **1990**, *92*, 5057–5086.

(34) Wang, Z.; Likhtman, A. E.; Larson, R. G. *Macromolecules* **2012**, *45*, 3557–3570.

(35) Everaers, R.; Sukumaran, S. K.; Grest, G. S.; Svaneborg, C.; Sivasubramanian, A.; Kremer, K. *Science* **2004**, *303*, 823–826.

(36) Limbach, H.; Arnold, A.; Mann, B.; Holm, C. *Computer Physics Communications* **2006**, *174*, 704 – 727.

(37) Auhl, R.; Everaers, R.; Grest, G. S.; Kremer, K.; Plimpton, S. J. *The Journal of Chemical Physics* **2003**, *119*, 12718–12728.

(38) Bačová, P.; Hawke, L. G. D.; Read, D. J.; Moreno, A. J. *Macromolecules* **2013**, *46*, 4633–4650.

(39) Read, D. J.; Jagannathan, K.; Sukumaran, S. K.; Auhl, D. *Journal of Rheology* **2012**, *56*, 823–873.

(40) Viovy, J. L.; Rubinstein, M.; Colby, R. H. *Macromolecules* **1991**, *24*, 3587–3596.

(41) Likhtman, A. E.; McLeish, T. C. B. *Macromolecules* **2002**, *35*, 6332–6343.

(42) Lentzakis, H.; Vlassopoulos, D.; Read, D. J.; Lee, H.; Chang, T.; Driva, P.; Hadjichristidis, N. *Journal of Rheology* **2013**, *57*, 605–625.

(43) Larson, R. G.; Sridhar, T.; Leal, L. G.; McKinley, G. H.; Likhtman, A. E.; McLeish, T. C. B. *Journal of Rheology* **2003**, *47*, 809–818.

(44) Fetters, L. J.; Lohse, D. J.; Richter, D.; Witten, T. A.; Zirkel, A. *Macromolecules* **1994**, *27*, 4639–4647.

(45) Roovers, J.; Graessley, W. W. *Macromolecules* **1981**, *14*, 766–773.

(46) Auhl, D.; Ramirez, J.; Likhtman, A. E.; Chambon, P.; Fernyhough, C. *Journal of Rheology* **2008**, *52*, 801–835.

(47) Liu, C.; He, J.; van Ruymbeke, E.; Keunings, R.; Bailly, C. **2006**, *47*.

(48) Snijkers, F.; Vlassopoulos, D.; Lee, H.; Yang, J.; Chang, T.; Driva, P.; Hadjichristidis, N. *Journal of Rheology* **2013**, *57*, 1079–1100.

(49) Rubinstein, M.; Colby, R. H. *Polymer physics.*; Oxford: Oxford University Press, 2003.

(50) Macosko, C. W. *Rheology: Principles, Measurements, and Applications.*; Wiley-VCH, NY, 1994.

(51) Roovers, J. *Macromolecules* **1984**, *17*, 1196–1200.

(52) Stephanou, P. S.; Baig, C.; Tsolou, G.; Mavrantzas, V. G.; Kröger, M. *The Journal of Chemical Physics* **2010**, *132*, 124904.

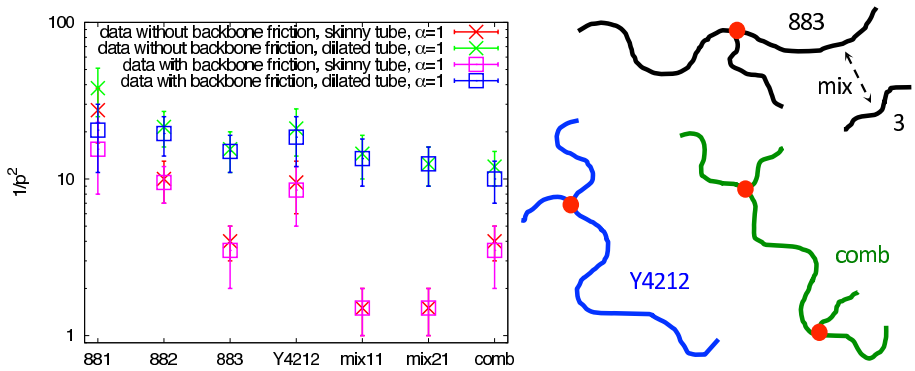

For Table of Contents use only

Title: “Branchpoint motion in architecturally complex polymers: estimation of hopping parameters from computer simulations and experiments”

Authors: Petra Bačová, Helen Lentzakis, Daniel J. Read, Angel J. Moreno, Dimitris Vlassopoulos and Chinmay Das